ANL/RTR/TM-15/10

Preliminary Results of Ancillary Safety Analyses Supporting TREAT LEU Conversion Activities

Nuclear Engineering Division

About Argonne National Laboratory

Argonne is a U.S. Department of Energy laboratory managed by UChicago Argonne, LLC under contract DE-AC02-06CH11357. The Laboratory's main facility is outside Chicago, at 9700 South Cass Avenue, Argonne, Illinois 60439. For information about Argonne and its pioneering science and technology programs, see www.anl.gov.

DOCUMENT AVAILABILITY

Online Access: U.S. Department of Energy (DOE) reports produced after 1991 and a growing number of pre-1991 documents are available free via DOE's SciTech Connect (http://www.osti.gov/scitech/)

Reports not in digital format may be purchased by the public from the National Technical Information Service (NTIS):

U.S. Department of Commerce
National Technical Information
Service 5301 Shawnee Rd
Alexandria, VA 22312
www.ntis.gov
Phone: (800) 553-NTIS (6847) or
(703) 605-6000
Fax: (703) 605-6900
Email: orders@ntis.gov

Reports not in digital format are available to DOE and DOE contractors from the Office of Scientific and Technical Information (OSTI):

U.S. Department of Energy
Office of Scientific and Technical Information
P.O. Box 62
Oak Ridge, TN 37831-0062
www.osti.gov
Phone: (865) 576-8401
Fax: (865) 576-5728
Email: **reports@osti.gov**

Disclaimer

This report was prepared as an account of work sponsored by an agency of the United States Government. Neither the United States Government nor any agency thereof, nor UChicago Argonne, LLC, nor any of their employees or officers, makes any warranty, express or implied, or assumes any legal liability or responsibility for the accuracy, completeness, or usefulness of any information, apparatus, product, or process disclosed, or represents that its use would not infringe privately owned rights. Reference herein to any specific commercial product, process, or service by trade name, trademark, manufacturer, or otherwise, does not necessarily constitute or imply its endorsement, recommendation, or favoring by the United States Government or any agency thereof. The views and opinions of document authors expressed herein do not necessarily state or reflect those of the United States Government or any agency thereof, Argonne National Laboratory, or UChicago Argonne, LLC.

ANL/RTR/TM-15/10

Preliminary Results of Ancillary Safety Analyses Supporting TREAT LEU Conversion Activities

prepared by
A. J. Brunett, T. Fei, P. S. Strons, D. D. Papadias, E. A. Hoffman, D. C. Kontogeorgakos, H. M. Connaway, A. E. Wright
Nuclear Engineering Division, Argonne National Laboratory

sponsored by
U. S. Department of Energy, National Nuclear Security Administration
Office of Material Management and Minimization

October 2015

Executive Summary

The Transient Reactor Test Facility (TREAT), located at Idaho National Laboratory (INL), is a test facility designed to evaluate the performance of reactor fuels and materials under transient accident conditions. The facility, an air-cooled, graphite-moderated reactor designed to utilize fuel containing high-enriched uranium (HEU), has been in non-operational standby status since 1994. Currently, in support of the missions of the Department of Energy (DOE) National Nuclear Security Administration (NNSA) Material Management and Minimization (M3) Reactor Conversion Program, a new core design is being developed for TREAT that will utilize low-enriched uranium (LEU). The primary objective of this conversion effort is to design an LEU core that is capable of meeting the performance characteristics of the existing HEU core. Minimal, if any, changes are anticipated for the supporting systems (e.g. reactor trip system, filtration/cooling system, etc.); therefore, the LEU core must also be able to function with the existing supporting systems, and must also satisfy acceptable safety limits.

In support of the LEU conversion effort, a range of ancillary safety analyses are required to evaluate the LEU core operation relative to that of the existing facility. These analyses cover neutronics, shielding, and thermal hydraulic topics that have been identified as having the potential to have reduced safety margins due to conversion to LEU fuel, or are required to support the required safety analyses documentation. The majority of these ancillary tasks have been identified in [1] and [2]. The purpose of this report is to document the ancillary safety analyses that have been performed at Argonne National Laboratory during the early stages of the LEU design effort, and to describe ongoing and anticipated analyses.

For all analyses presented in this report, methodologies are utilized that are consistent with, or improved from, those used in analyses for the HEU Final Safety Analysis Report (FSAR) [3]. Depending on the availability of historical data derived from HEU TREAT operation, results calculated for the LEU core are compared to measurements obtained from HEU TREAT operation. While all analyses in this report are largely considered complete and have been reviewed for technical content, it is important to note that all topics will be revisited once the LEU design approaches its final stages of maturity. For most safety-significant issues, it is expected that the analyses presented here will be bounding, but additional calculations will be performed as necessary to support safety analyses and safety documentation. It should also be noted that these analyses were completed as the LEU design evolved, and therefore utilized different LEU reference designs.

Preliminary shielding, neutronic, and thermal hydraulic analyses have been completed and have generally demonstrated that the various LEU core designs will satisfy existing safety limits and standards also satisfied by the existing HEU core. These analyses include the assessment of the dose rate in the hodoscope room, near a loaded fuel transfer cask, above the fuel storage area, and near the HEPA filters. The potential change in the concentration of tramp uranium and change in neutron flux reaching instrumentation has also been assessed. Safety-significant thermal hydraulic items addressed in this report include thermally-induced mechanical distortion of the grid plate, and heating in the radial reflector.

Table of Contents

Page

Executive Summary ..... **i**

Table of Contents ..... **iii**

List of Figures ..... **v**

List of Tables ..... **vii**

Acronyms ..... **viii**

1. Introduction **10**

2. Overview of TREAT **12**

3. Shielding and Neutronic Analyses **15**

3.1 HEU vs. LEU Comparison of Tramp Uranium and Dose Rate at HEPA Filters 15
3.1.1 Quantity of tramp uranium 15
3.1.2 Operating History 16
3.1.3 Estimating Source Term 16
3.1.4 Estimating Dose Rate from HEPA Filters 18
3.1.5 Conclusion 18
3.2 Photon Dose Rate Evaluation in the Hodoscope Room 18
3.2.1 Methodology 19
3.2.2 Results 21
3.3 Photon Dose Rate Evaluation Around a Loaded TREAT Fuel Transfer Cask 22
3.3.1 Methodology 22
3.3.2 Results 25
3.4 Photon Dose Rate Evaluation Above the Storage Area 26
3.4.1 Methodology 26
3.4.2 Results 28
3.5 Comparison of Neutron Fluxes at Detectors in M8CAL 28
3.5.1 MCNP Calculations 29
3.5.2 Conclusion 29

4. Thermal Hydraulic Analyses **31**

4.1 Heat Transfer From Test Vehicle to Core 31
4.2 Thermal Hydraulic Analysis of the Permanent Reflector and Core Support 33
4.2.1 Geometrical Domain 34
4.2.2 Model and Methodology 36
4.2.3 Scope of analysis 39
4.2.4 Results 40
4.2.5 Summary 44
4.3 Grid Plate Thermal Distortion 45
4.3.1 Assumptions 45
4.3.2 Non-Uniform Thermal Loading 46
4.3.3 Maximum Uniform Temperature 50
4.3.4 Summary 52

5. Ongoing and Future Ancillary Safety Analyses **54**
6. Conclusions **56**
Works Cited **57**
Appendix A **59**

List of Figures

Page
Figure 1: Side Cut-Away View of TREAT 13
Figure 2: Plan View of TREAT 14
Figure 3: MCNP6 Model for the Shielding Calculation of Photon Dose Rate in the Hodoscope Room ... 20
Figure 4: Photon Flux (photons/cm^2-s/source) Distribution Between the Photon Source and the Hodoscope Room 21
Figure 5: TREAT Cask Model in Horizontal (left) and Vertical (right) Plane 23
Figure 6: Photon Dose Rate Distribution Around a TREAT Cask 26
Figure 7: The MCNP6 Model of the Storage Area in Horizontal (left) and Vertical (right) Plane 27
Figure 8: Configuration of the Instrumentation in the TREAT Core 28
Figure 9: Perspective View of TREAT [6] 34
Figure 10: Drawing of a Quarter Section of the Core Grid Support Plate [5] 35
Figure 11: a) Schematic Cross-Section of TREAT, b) Four neighboring fuel assemblies form a cooling passage 36
Figure 12: Schematic of Permanent Reflector and Flow Regions 37
Figure 13: Grid Plate Configuration for M8CAL (without Fuel Alignment Pins) 38
Figure 14: Section of the Grid Plate Showing: A) Fuel alignment hole, B) Fuel alignment pin, C) Fuel alignment pin attached to grid plate section 39
Figure 15: Maximum Peak Temperature History of the Permanent Reflector for the LEU Core as a Function of Cooling Rate 41
Figure 16: Maximum Grid Plate Temperature Profiles During a Reactivity Accident Scenario 42
Figure 17: Temperature Profiles as a Function of Time and Energy Deposited in the Fuel Assemblies for the Assumed LEU Core. a) Gas phase temperatures exiting the cooling channels, b) Temperature of the alignment pin, c) Average temperatures entering the radial slots of the grid plate (see Figure 13 for location) 43
Figure 18: Reactor Effluent Air to the Exhaust Filtration System 44
Figure 19: Drawing of Grid Plate and Seal Assemblies 46
Figure 20: Cross-Sectional View of Control Rod Assembly Showing Graphite Bearings (Red) 47
Figure 21: Non-Thermal Grid Plate Loads in the Quarter Symmetry Model 48
Figure 22: Contour Plot of Non-Uniform Thermal Loading of the Grid Plate in the Design Basis Accident [28] 48
Figure 23: Contour Plots Showing Total (a) and Radial (b) Deformation of the Grid Plate Due to Non-Uniform Thermal Loading 49
Figure 24: Deflection of Control Rod Positions 50
Figure 25: Control Rod Deflection Resulting from 0.31° Angular Displacement at Middle Bearing 50
Figure 26: Contour Plot Showing Uniform Grid Plate Temperature of 320 °C 51
Figure 27: Radial Deformation (a) and Total Deflection (b) Resulting From Uniform Thermal Load of 320°C 52
Figure 28: Control Rod Deflection Resulting from 0.443° Angular Displacement at Middle Bearing 52
Figure A - 1: Cross-Section View of MCNP Model of the M8CAL Experiment Core Loading [25] 59
Figure A - 2: Fraction of Core Energy Deposition for an Accident Scenario (5.20% reactivity insertion). Total core energy during the transient: HEU = 4.6 GJ, LEU = 5.59 GJ [29]. 60

Figure A - 3: Grid Plate Temperature Profiles for HEU core During Steady State Power Operation at 120 kW, Air Coolant Flow Rate = 3000 cfm 61
Figure A - 4: Grid Plate Temperature Profiles for LEU Core (Variant 2.1) During Steady State Power Operation at 120 kW, Air Coolant Flow Rate = 3000 cfm 62

List of Tables

Page
Table 1: Corresponding LEU Design Variant and Reference HEU FSAR Section for Ancillary Safety Analyses 11
Table 2: Normalized Spectra of Photon Sources Accumulated in the HEPA Filter [9] 20
Table 3: Results Comparison Between the Current Model and the Model from Ref. [11] 22
Table 4: Nuclide Activities Over All Burnable Zones in TREAT After 20 Years of Operation 24
Table 5: Power History of TREAT 24
Table 6: Photon Energy Spectrum in the Fuel Region of a Discharged Fuel Subassembly 25
Table 7: Photon Dose Rate Outside the Cask 25
Table 8: Photon Energy Spectrum in the Fuel Region of a Discharged Fuel Assembly 27
Table 9: Photon Dose Rate Above Storage Area 28
Table 10: LEU/HEU Ratio of the Thermal and Total Neutron Flux Reaching the Detectors' Location 29
Table 11: Thermal to Total Neutron Flux Calculated with MCNP for the HEU and the LEU Cores 29
Table 12: Material Properties for A36 Steel 46

Acronyms

DOE	Department of Energy
DBA	Design Basis Accident
FSAR	Final Safety Analysis Report
HEU	High-enriched Uranium
ICRP	International Commission on Radiological Protection
INL	Idaho National Laboratory
ID	Inner Diameter
LEU	Low-enriched Uranium
NNSA	National Nuclear Security Administration
PCF	Power Coupling Factor
TED	Total Energy Deposition
TREAT	Transient Reactor Test Facility
TU	Tramp Uranium

1. Introduction

The Transient Reactor Test Facility (TREAT), located at Idaho National Laboratory (INL), is a test facility designed to evaluate the performance of reactor fuels and materials under transient accident conditions. The facility, an air-cooled, graphite-moderated reactor designed to utilize fuel containing high-enriched uranium (HEU), has been in non-operational standby status since 1994. Currently, in support of the missions of the Department of Energy (DOE) National Nuclear Security Administration (NNSA) Reactor Conversion Program, a new core design is being developed for TREAT that will utilize low-enriched uranium (LEU). The primary objective of this conversion effort is to design an LEU core that is capable of meeting the performance characteristics of the existing HEU core. Minimal, if any, changes are anticipated for the supporting systems (e.g. reactor trip system, filtration/cooling system, etc.); therefore, the LEU core must also be able to function with the existing supporting systems, and must also satisfy the general safety criteria established for the HEU core with sufficient margin.

In support of the LEU conversion effort, a range of ancillary safety analyses are required to ensure the LEU core operates within the envelope of the existing facility. These analyses cover neutronic, shielding, and thermal hydraulic topics that have been identified as having the potential to have reduced safety margin due to conversion to LEU fuel, or are required to support the required safety analyses documentation. The majority of these ancillary tasks have been identified in [1] and [2]. The purpose of this report is to document the ancillary safety analyses that have been completed at Argonne National Laboratory during the early stages of the LEU design effort, and to describe ongoing and anticipated analyses.

For all analyses presented in this report, methodologies are utilized that are consistent with, or improved from those used in analyses for the HEU Final Safety Analysis Report (FSAR) [3]. Depending on the availability of historical data derived from HEU TREAT operation, results calculated for the LEU core are compared to measurements obtained from HEU TREAT operation. For all analyses, the corresponding section in the FSAR has been identified and can be found in the text of each section and in Table 1. While all analyses in this report are largely considered complete and have been reviewed for technical content, it is important to note that all topics will be revisited once the LEU design approaches its final stages of maturity. For most safety-significant issues, it is expected that the analyses presented here will be bounding, but additional calculations will be performed as necessary to support safety analyses and safety documentation.

It should also be noted that these analyses were completed as the LEU design evolved, and therefore utilized different LEU reference designs. For each analysis in this report, the LEU design iteration is identified in the text of each section and in Table 1. A description of the LEU design variants, including Baseline 2.0, can be found in [4].

Table 1: Corresponding LEU Design Variant and Reference HEU FSAR Section for Ancillary Safety Analyses

Analysis Topic	Report Section	LEU Design	HEU FSAR Section
HEU vs. LEU Comparison of Tramp Uranium and Dose Rate at HEPA Filters	3.1	Baseline 2.0	12.3.2.4
Photon Dose Rate Evaluation in Hodoscope Room	3.2	Baseline 2.0	12.3.2.4
Photon Dose Rate Evaluation Around a Loaded TREAT Fuel Transfer Cask	3.3	Baseline 2.0	9.5.2
Photon Dose Rate Evaluation Above the Storage Area	3.4	Baseline 2.0	9.5.1, 12.3.2.2
HEU vs. LEU Comparison of Neutron Fluxes at Detectors	3.5	Variant 2.1	3.1.2 (GDC-13), 7.2, 7.7
Heat Transfer from Test Vehicle to Core	4.1	-	15.10.1.G
Heating in the Permanent Reflector and Core Support	4.2	Variant 2.1	4.3.2.2, 4.3.6, 15.3.2.3, 15.9
Grid Plate Thermal Distortion	4.3	Variant 2.1	4.3.2.4, 4.5.6.4

This report begins with a high-level overview of the configuration of TREAT in Section 2. Section 3 provides a description of the shielding and neutronic ancillary safety analyses that have been completed as of the conclusion of FY15. These analyses include dose rate evaluations at the HEPA filters (Section 3.1), in the hodoscope room (Section 3.2), near a loaded fuel transfer cask (Section 3.3), and above the storage area (Section 3.4). A comparison of the flux at detectors between the HEU and LEU cores is also provided in (Section 3.5). Thermal hydraulic and structural analyses are discussed in Section 4; these topics include heat transfer from the test vehicle to the core (Section 4.1), heating of the permanent reflector and grid plate (Section 4.2), and mechanical distortion of the grid plate (Section 4.3). In-progress and planned safety analyses are discussed in Section 5, and concluding remarks are provided in Section 6.

2. Overview of TREAT

This section provides a high-level overview of the configuration of TREAT; more details of the reactor and facility can be found in [5] [6] [7]. TREAT, a homogeneous, air-cooled, graphite–reflected reactor, is currently fueled with 93% enriched UO_2 distributed in a graphite moderator matrix, where the carbon-to-U^{235} ratio ($C:U^{235}$) is approximately 10000:1. The 19x19 fuel array consists of 4-in square assemblies, with an active fuel length of 4ft located between two 2-ft upper and lower graphite reflectors. The reflector sections of the fuel assemblies are enclosed in 50-mil-thick type 1100 aluminum cladding, whereas the fueled region is evacuated and sealed with 25-mil-thick Zircaloy-3 cladding. Experiments are accommodated by replacing two to four fuel assemblies at the radial center of the core with a test vehicle containing the samples to be irradiated. Control of the reactor is accomplished via three types of bottom-inserted B_4C control rods: four pairs of control/shutdown rods to drive criticality, four pairs of transient rods used for transient tests and rapid reactivity insertion, and four compensation rods primarily used for reactivity makeup in the absence of experiment vehicles. Control rod drives are located in the subpile room below the core.

A permanent radial reflector surrounds TREAT. It is comprised of 4-in square blocks stacked such that the reflector has an approximate height of 7.75 ft and thickness of 2 ft. Cooling of the reflector is accommodated for by a 2-in gap on the interior and exterior of the reflector that allows air flow between the fuel and reflector, and reflector and concrete shield. Removable shielding blocks that penetrate the concrete shield on the north, west, and south faces allow for the use of detectors and ex-vessel experiment imaging/visualization tools, such as the hodoscope and radiography facility. Concrete removable blocks above the active core provide access to the fuel matrix for fuel and experiment handling. With the exception of the penetrating viewing slots, the concrete shield has a thickness of 5 ft. A side perspective of the facility is shown in Figure 1, and a plan view is shown in Figure 2.

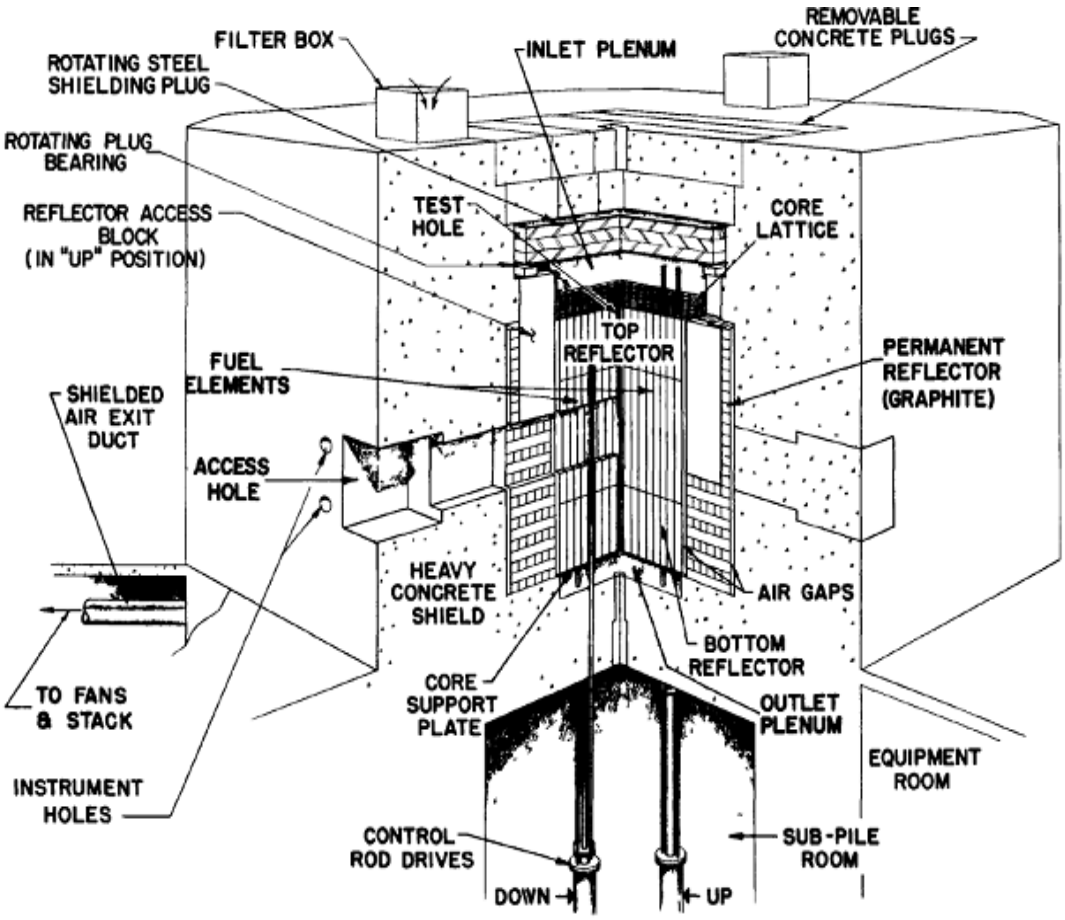

Figure 1: Side Cut-Away View of TREAT

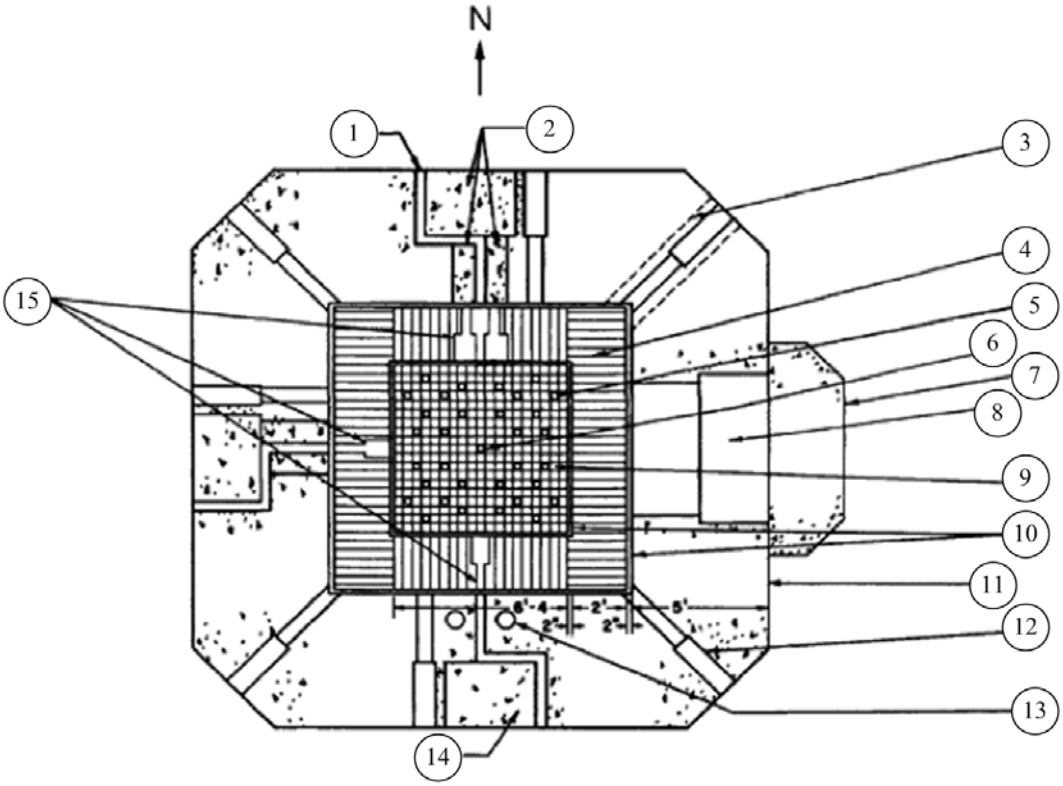

Item No.	Description	Item No.	Description
1	Access Hole	9	Core Lattice
2	Removable Shielding Blocks	10	Air Gaps
3	Air Exit Duct	11	Heavy Concrete Shield
4	Permanent Graphite Reflector	12	Typical Instrument Holes
5	Control Rods	13	Return Ducts for In-Pile Loop
6	Test Hole	14	Removable Shield Block
7	Thermal Column Shield Door	15	Reflector Access Blocks
8	Graphite Thermal Column		

Figure 2: Plan View of TREAT

3. Shielding and Neutronic Analyses

This section discusses the shielding and neutronic analyses completed in support of TREAT conversion efforts. These analyses are largely focused on ensuring that the risk to personnel from the LEU core does not exceed the risk presented by the HEU core and therefore also satisfies regulatory limits. An analysis of anticipated detector flux is also presented in this section, where the intent of this analysis is to demonstrate the compatibility and continued functionality of the existing detectors at TREAT. For all analyses presented here, methodologies are utilized that are consistent with, or improved from, those used in the HEU FSAR. Results calculated for the LEU core are compared to historical data obtained from HEU TREAT operation, when the data is available.

Ancillary analyses discussed in this section include analysis of tramp uranium (uranium that is permanently fixed on the external surface of fuel assemblies) and evaluation of dose rate at HEPA filters (Section 3.1) dose rate evaluation in the hodoscope room (Section 3.2), dose rate evaluation near a loaded fuel transfer cask (Section 3.3), dose rate evaluation above the storage area (Section 3.4), and comparison of flux at various detectors (Section 3.5).

While all of the analyses in this section are considered to be complete and have been reviewed for technical content, it should be noted that all topics will be revisited once the LEU design has achieved a final stage of maturity. In most cases, it is expected that the analyses presented here will act as bounding analyses, but additional calculations will be performed where the margin to satisfy the various safety criteria is not large.

3.1 HEU vs. LEU Comparison of Tramp Uranium and Dose Rate at HEPA Filters

Estimating the dose rate from fission products deposited in or near the HEPA filters as the result of tramp uranium is an extremely complex problem. The key variables are the actual quantity of tramp uranium in the cladding material, the fission history of that material, the transport and deposition of the fission products from the tramp uranium, and the deposition of the fission products or their daughters in the filters (i.e., the source term).

This analysis was completed using the Baseline 2.0 iteration of the LEU core design as a reference. This assessment is considered bounding for any core design that exhibits a lower or similar flux, with a similar photon spectrum. A description of similar analyses completed for the HEU core can be found in Section 12.3.2.4 of the HEU FSAR.

3.1.1 Quantity of tramp uranium

While a conservative estimate should be based on the impurity limit of uranium in the cladding material, a best estimate would be based on the actual value. Normal levels of impurities are often far below their limits. Specific data was not found on the normal range of tramp uranium impurities in Zircaloy. The commercial specification for Zircaloy-4 is <3.5 ppm [8].

For this analysis, the estimate of the dose rate in the TREAT facility due to tramp uranium in the TREAT core assemblies is based on scaling past measurements for the HEU core. Replacing that core with a LEU core, one key factor will be the relative concentration of the tramp uranium in the cladding of the assemblies. This data is currently unavailable. This is a large source of uncertainty since the source term will scale linearly with the concentration of tramp uranium. No data on the normal variation in impurity levels were available either. Without that information, significant uncertainty in the source term due to tramp uranium is expected.

The changes from the HEU core to an LEU core will not involve significant changes in the geometry (external surface area in particular) of the cladding in the active core region. The Zircaloy cladding is extended further outside of the active core region, but the much-lower flux in these regions will have a very small impact in the source term from the fission of tramp uranium.

3.1.2 Operating History

The dose rate will be a strong function of the operating history because it will have a large contribution from very-short-lived fission products. In addition, the accumulation of longer-lived fission products will be a significant contributor to occupational exposure. The short-lived isotopes will likely dominate the peak rate during and immediately after reactor transients, but, because they quickly decay away, the longer-lived isotopes will likely dominate the steady-state rate. The cumulative occupational dose will depend on when personnel are close to the filters in the area when the reactor is not operating, during steady-state reactor operation, and after reactor transients. It will also depend, of course, on the reactor operating history since the filters were last replaced.

Ideally, if the peak dose rate can be maintained below an acceptable occupational radiological limit for a conservative operating history, then most of the complexity can be disregarded in the analysis. So the first step in addressing this problem was to develop a reasonably-conservative estimate of the peak dose rates.

Replacing the HEU core with LEU will have some impact on the neutron spectrum and flux level at a given power level. This will impact the relative fission rate of the tramp uranium at a given power level. MCNP calculations were performed to estimate the relative fission rate of tramp uranium at the same core total power level for both the present HEU core and the Baseline 2.0 LEU core design. The computations estimated a 3% higher fission rate in the LEU core, assuming the tramp uranium concentration is the same in the LEU core as the HEU core. Given all the uncertainties in estimating the source term from the fission of tramp uranium, this is a negligible difference. The measured data from the HEU core can therefore be scaled for the LEU core by using the anticipated difference in power level during operation.

3.1.3 Estimating Source Term

The source term will naturally be time dependent and distributed throughout the entire air flow system of the reactor. The first step in evaluating the source term was to estimate the quantity of fission products that are released into the air flow system. The second step was to determine how those fission products will behave as they move through the system. This is greatly complicated by the fact that some of the fission products will change chemical form in transit because of radioactive decay.

3.1.3.1 Fission Product Release

The release of fission products from tramp uranium results from the recoil of the fission products after fission. If located at the surface of the cladding, one fission product will recoil into the coolant and the other fission product will recoil into the cladding. As the location of the fission moves inward from the cladding surface, the rate of release into the coolant will fall quickly. This is because the random direction of the fission product release will quickly reduce the solid angle over which a given fission product recoils with a track length to the surface less than the range of that fission product. The range of fission products is on the order of 50 Å and is a strong function of the fission product energy and the local material composition. Thankfully, there is empirical data available for TREAT that allows us to estimate the release rate for that fuel design. This can then be adjusted to the LEU fuel design.

R.W. Swanson estimated the annual radioactive emissions from the TREAT stack [9] based on measured release data. This estimate was for a 350,000 MJ annual energy production in the TREAT HEU core,

which corresponds to approximately 1.0E22 fissions per year in the core. In Table 1 of that memo, the annual radioactive emissions were estimated such that they were consistent with a significant number of actual measurements made at the TREAT stack. These values were then used to estimate the release rate of noble-gas fission products (krypton and xenon) into the air stream. This involved correcting for radioactive decay from the time of release from the point of fission into the air stream to the time the radiation was measured at the TREAT stack. Combining that information with the fission product yield, the fraction of fission products that recoil into the air due to fissioning of the tramp uranium was estimated. The release rate was determined to be on the order of 1.0E-5 (~0.8E-5 to 2.0E-5) times the total core fission rate. This is consistent with a previous estimate [10].

This estimate will then need adjustment for the LEU core. This includes accounting for the relative tramp uranium composition in the cladding of the LEU assemblies, if known. In addition, adjustments will be needed for differences in the relative cladding surface area and differences in flux level between the HEU and LEU cores, to correct for the fission rate of tramp uranium near the cladding surface relative to the fission rate in the core. These are likely to be small corrections relative to the overall uncertainty of the analysis.

3.1.3.2 Deposition of Fission Products

Combining the operating history and the estimated release fraction, both of which are challenging to estimate accurately, provides the source term of fission products that recoil into the air coolant. There are essentially two extremes for estimating the source term in the HEPA filter. The low estimate is that the solid fission products deposit in the coolant channels very close to the point of their formation. The high estimate is that they only deposit in the HEPA filter. A previous analysis estimated a value of 320 mr/hr, which is at least two orders of magnitude larger than the actual measurements [11]. The basis for the 320 mr/hr appears to be the assumption that all fission products produced by tramp uranium [10] are included in the estimate of the dose rate, which is consistent with the high estimate obtained by assuming all of the material is deposited in the HEPA filter.

The physics seem to suggest that extremely small particles (e.g., single atoms of solid fission products) would not travel very far before depositing on a surface because Brownian motion would cause them to impact a surface before they have moved very far. The velocity of particles relative to the average velocity of air through the core is very large for smaller particles, meaning there is a high probability of impact with structures due to Brownian motion. For relatively large particles, the velocity may be lower, but momentum causes deposition at bends and corners in the air flow channel. As the result of these two mechanisms, most particles would be deposited on the fuel-assembly cladding near the point of fission rather than in the HEPA filter. Daughter products, from noble-gas decay, that would be deposited in or near the HEPA filter would only be those generated by noble gas decay flowing in the air stream in or near the HEPA filter.

Two calculations were performed. The first was for a brief irradiation, and the source term of all fission products was calculated as a function of time. The second was for the same brief irradiation, followed by a short decay based on the transit time of the coolant from the core to the HEPA filter (~ 15 seconds), assuming everything but the noble-gas fission products were removed, then the noble gases are allowed to decay for a short time (5 seconds), and the source term for the daughters of the noble gas was calculated. This quick calculation suggests a roughly two orders of magnitude of reduction in source strength between all fission products and the daughters of the noble-gas fission products. This will be confirmed

with more-thorough analysis if necessary, but the results seem consistent with limited transport of all fission products from the tramp material except the noble gases in the coolant.

3.1.4 Estimating Dose Rate from HEPA Filters

It is impractical to develop a first-principles estimate of the dose rate from the fission products produced by the fission of tramp uranium in the cladding depositing in the HEPA filters. A parametric approximation can be made based on the understanding of the processes. Equation (1) is for a transient, and equation (2) is for steady state operation.

$$\dot{D}_{LEU,transient} = \alpha_{HEU,transient,measured} \frac{E_{LEU,transient}}{E_{HEU,transient}} \frac{\left(\sigma_{fis,NU}\phi\right)_{LEU}}{\left(\sigma_{fis,NU}\phi\right)_{HEU}} \frac{C_{TU,LEU}}{C_{TU,HEU}} \frac{S_{eff,LEU}}{S_{eff,HEU}} \tag{1}$$

$$\dot{D}_{LEU,steadystate} = \alpha_{HEU,steadystate,measured} \frac{P_{LEU,steadystate}}{P_{HEU,steadystate}} \frac{\left(\sigma_{fis,NU}\phi\right)_{LEU}}{\left(\sigma_{fis,NU}\phi\right)_{HEU}} \frac{C_{TU,LEU}}{C_{TU,HEU}} \frac{S_{eff,LEU}}{S_{eff,HEU}} \tag{2}$$

These equations involve the estimates based on measured data [11]. This data is scaled by four terms. The first is the relative energy or power level for the transient or steady state operation. The second term is the estimated ratio of fission rate for natural uranium (tramp uranium) in the LEU core relative to the HEU core. This ratio was estimated at 1.03 [12]. The third term is the ratio of TU density in the LEU cladding to that in the HEU cladding. No information was found to estimate this term or its likely range. The last term is the ratio of effective cladding surface area between the two cores. While the LEU core will have Zircaloy cladding that extends outside of the active core region, the much-lower flux level outside the core will not result in a large source term from this region, so this final ratio should be approximately 1.0.

Except for the unknown concentration, the dose rate should scale linearly with the energy or power level, with the impact of the design changes being small compared to the uncertainty.

3.1.5 Conclusion

Past calculations and measured data suggest a maximum dose rate of around 1 mr/hr at the mezzanine area near the TREAT reactor due to the HEPA filter source [11]. It seems unlikely that this value will change significantly with the LEU-fueled core or that a much-improved practical method deriving an estimate could be made. The one area of concern is whether or not significant variation in the tramp uranium concentration is likely between the Zircaloy used for the HEU core and the Zr-bearing material to be selected for the LEU core. No information was found on the normal variation among zirconium alloys. The difference in tramp uranium fission rate per unit of core power generation in the LEU core was determined to be only slightly (3%) greater than in the HEU core. For reactor operations in which a certain amount of fission power generation in experiment fuel is necessary, the required amount of LEU core power and energy will be different from the required amount of HEU core power and energy. This LEU/HEU energy ratio will proportionally affect the amount of tramp uranium fissions generated during such operations.

3.2 Photon Dose Rate Evaluation in the Hodoscope Room

During the operation of TREAT, tramp uranium in the cladding of the fuel elements undergo fissions and releases fission product particles into the coolant. These fission product particles accumulate in the HEPA filters and emit high-energy photons. Because personnel typically need to enter and work within the hodoscope room soon after transients are performed, a shielding calculation was performed to evaluate

the photon dose rate in the hodoscope room due to these photon sources accumulated in the HEPA filters. This analysis uses information derived from the calculations described in 3.1.

The analysis was completed using the Baseline 2.0 iteration of the LEU core design as a reference. This assessment is considered bounding for any core design that exhibits a lower or similar flux, with a similar photon spectrum. A description of similar analyses completed for the HEU core can be found in Section 12.3.2.4 of the HEU FSAR.

3.2.1 Methodology

The Monte Carlo code MCNP6 [13] was employed to perform the shielding calculation. The photon source strength and energy spectrum of fission products accumulated in the HEPA filter for the HEU core were obtained from Ref. [14] and [10]. The photon source strength is in the range of 1.0E9 to 1.0E11 photons/s according to Ref. [14], which is derived from two assumptions. The first assumes all the fission products produced by the tramp uranium (TU) would be collected in the HEPA filter, which gives a higher photon emitting rate (1.0E11 photons/s). The second assumes that only noble gases (Xe, Kr) released from fission can reach the HEPA filter. Thus, only the decay products of the noble gases would be collected in the HEPA filter. The isotropic angular photon source strength (1.0E9 photons/s) calculated based on the second assumption was significantly smaller than that predicted with the first assumption. The photon source strength from Ref. [10] was about 2.74E11 photons/s, which also conservatively assumed that all fission products generated by tramp uranium would deposit in the HEPA filter bank. For these calculations, it was assumed that the concentration of TU is the same in the LEU core as in the HEU core. Based on the neutronic evaluations of core performance for the Baseline 2.0 core [4], the LEU core was expected to operate at 25% higher power and energy than that of HEU core. The fission rate would thus be higher by 25%, and the total photon source in the HEPA filter would be increased by 25% to 3.43E11 photons/s, which was used to normalize the MCNP6 results.

The photon spectra obtained from Ref. [14] are listed in Table 2 for both assumptions discussed above.

The shielding layout for the hodoscope room was obtained from Ref. [11]. The MCNP6 model for the layout is presented in Figure 3. In general, there are 2” lead and 12” concrete shields between the source in the HEPA filter and the hodoscope room (located at the bottom left corner of the figure).

Table 2: Normalized Spectra of Photon Sources Accumulated in the HEPA Filter [14]

Energy (Mev)	Noble Gas	All Fission Products
0.01	2.13E-01	2.35E-01
0.03	4.31E-02	6.41E-02
0.04	2.84E-02	4.47E-02
0.06	4.14E-02	4.80E-02
0.09	2.54E-02	3.68E-02
0.13	1.74E-02	3.84E-02
0.23	3.36E-02	9.00E-02
0.38	1.42E-02	6.45E-02
0.58	2.84E-01	1.13E-01
0.85	1.15E-01	1.24E-01
1.25	1.78E-01	8.09E-02
1.75	3.10E-03	2.18E-02
2.25	1.45E-03	2.44E-02
2.75	1.01E-03	1.14E-02
3.50	1.28E-04	3.97E-03
5.00	5.95E-06	2.51E-05
7.00	0.00E+00	9.74E-28
9.50	0.00E+00	6.17E-29

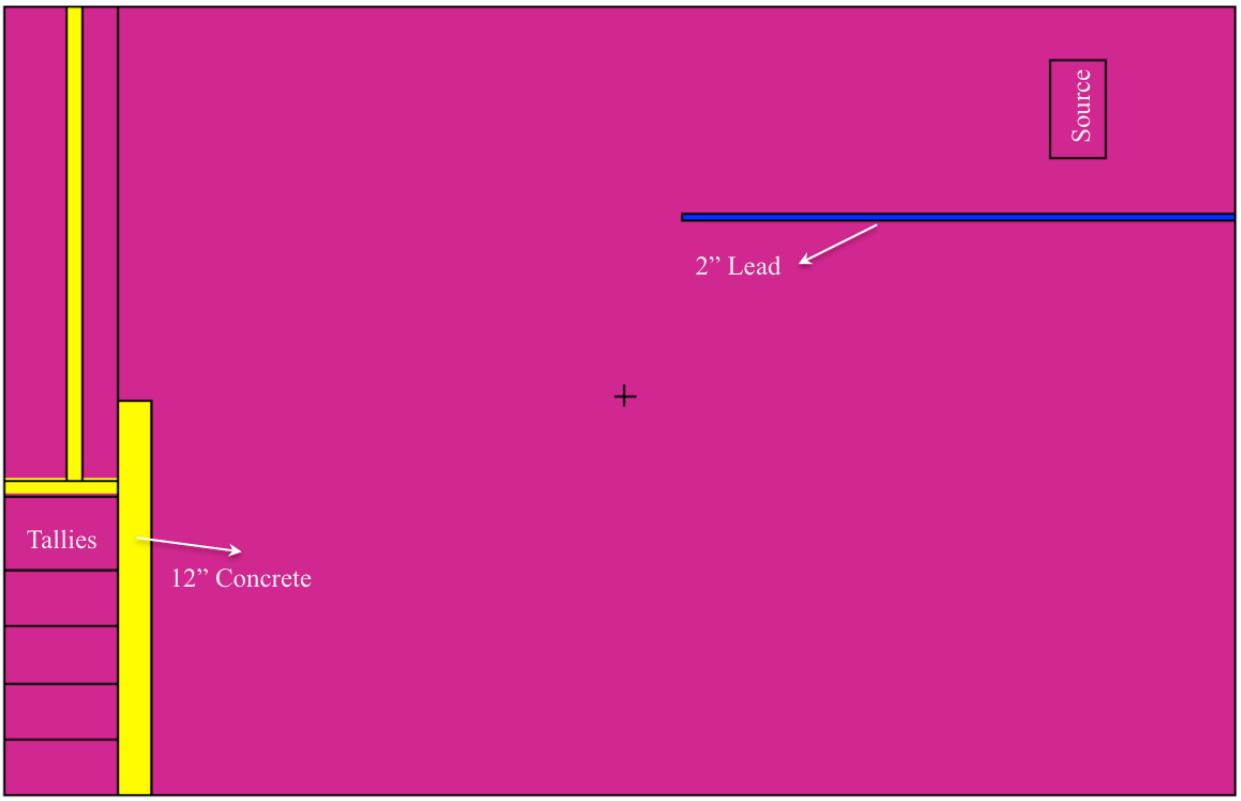

Figure 3: MCNP6 Model for the Shielding Calculation of Photon Dose Rate in the Hodoscope Room

3.2.2 Results

The photon dose rate in the hodoscope room for the LEU core is calculated as roughly 1.02E-2 mrem/hr, with a statistical uncertainty of 5.15%. This value was obtained based on the assumption that all fission products of tramp uranium were collected in the HEPA filter. The dose rate would be 100 times smaller if only the decay products of noble gases were collected in the HEPA filter.

The photon flux distribution is plotted in Figure 4. It shows that the combination of the lead shield and the concrete shield is able to significantly reduce the number of photons that can reach the hodoscope room.

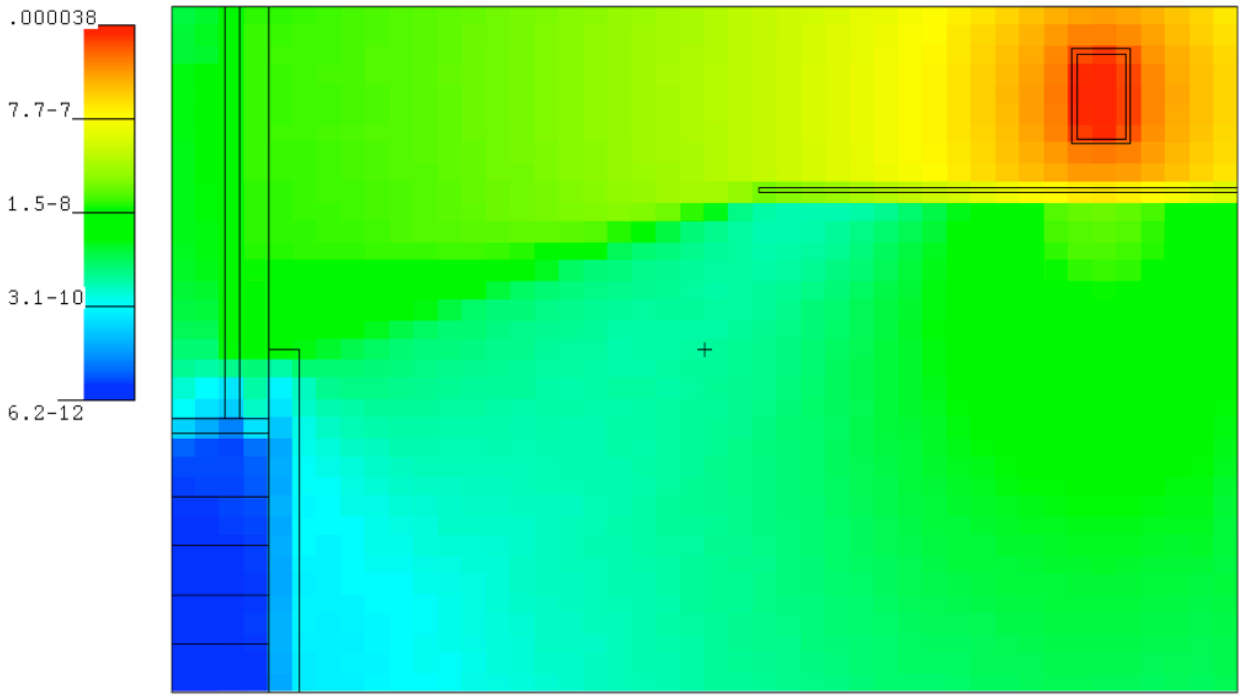

Figure 4: Photon Flux (photons/cm^2-s/source) Distribution Between the Photon Source and the Hodoscope Room

The evaluated dose rate in the hodoscope room was compared with that calculated in Ref. [11] for the HEU core. The results are listed in Table 3. A large difference was observed between the results calculated from the current model and the data in Ref. [11]. A series of simplified calculations were therefore performed to investigate the origin of the difference. The simplified model consisted of a point source in spherical shells made of shields. The dose rate was evaluated 10 m away from the point source and normalized by the source strength of 2.74E11 photons/s. The Spherical Case 1 is similar to the configuration assumed in the Ref. [11] model, and this simulation predicted a dose rate (2.08 mrem/hr) on the same order as that predicted in Ref. [11]. This dose rate was reduced to 0.85 mrem/hr when using the actual shield (2” lead + 12” concrete), and was further reduced to 0.08 mrem/hr when changing the photon spectrum to that listed in the third column of Table 2. Thus, the large difference in the results obtained from the current LEU model and Ref. [11] is caused by the difference in the geometry, the shielding material, and the source spectrum.

Table 3: Results Comparison Between the Current Model and the Model from Ref. [11]

Cases	Shield	Photon Spectrum	Dose Rate (mrem/hr)
Ref. [11] model	6” steel	Gamma source (1 – 3 MeV)	6.1
Current model	2” lead + 12” concrete	Table 2 Column 3	8.17E-03
Spherical Case 1	6” steel	Gamma source (1 – 3 MeV)	2.08
Spherical Case 2	2” lead + 12” concrete	Gamma source (1 – 3 MeV)	0.85
Spherical Case 3	2” lead + 12” concrete	Table 2 Column 3	0.08

3.3 Photon Dose Rate Evaluation Around a Loaded TREAT Fuel Transfer Cask

The photon dose rate was evaluated outside a TREAT Fuel Transfer Cask that is loaded with a TREAT fuel assembly. The radiation dose limit was obtained from two sources, and the more restrictive limit was utilized. In the United States Code of Federal Regulations (10 CFR § 20) [15], the annual occupational limit of the total effective dose equivalent is 5 rem. The International Commission on Radiological Protection (ICRP) [16] recommends the annual occupational dose to be 50 mSv (5 rem) and limits the dose received over five -year period to below 100 mSv (10 rem).

This analysis was completed using the Baseline 2.0 iteration of the LEU core design as a reference. This assessment is considered bounding for any core design that exhibits a lower or similar flux, with a similar photon spectrum. A description of similar analyses completed for the HEU core can be found in Section 9.5.2 of the HEU FSAR.

3.3.1 Methodology

The Monte Carlo code MCNP6 [13] was employed to perform the shielding calculation. The weight window variance reduction technique was used to ensure the calculation could be completed in a reasonable time. The cask model is presented in Figure 5 in both horizontal and vertical planes. One discharged fuel assembly was located in the cask. The assembly features an approximately 4-ft-long fuel section of 19.75% enriched UO_2-graphite fuel with a carbon-to-uranium atom ratio of approximately 1500:1, with roughly 2-ft-long graphite axial reflectors above and below the fuel. Additional details on the fuel design can be found in [4].

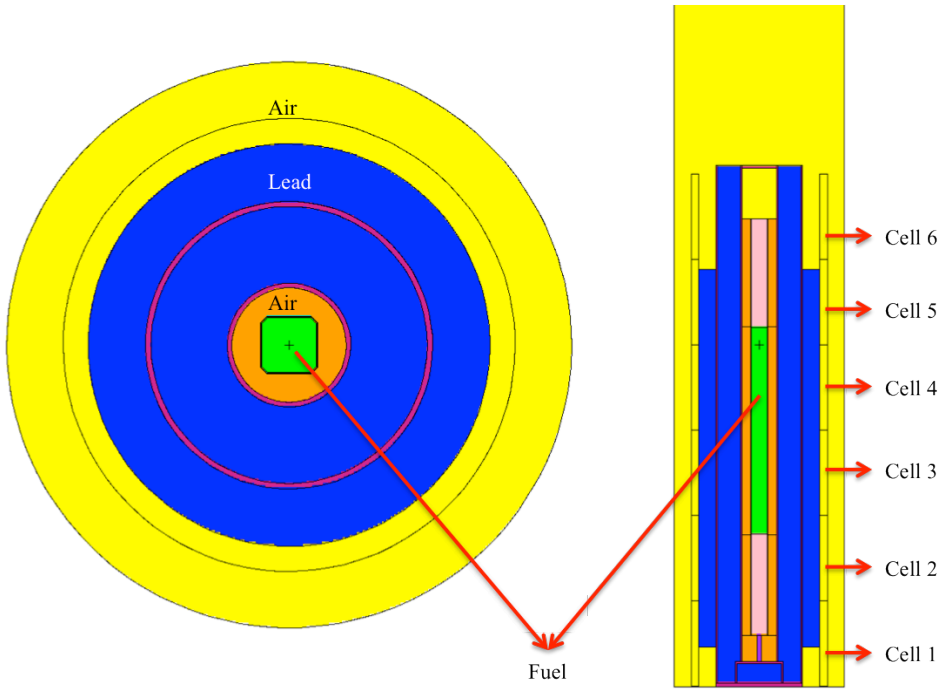

Figure 5: TREAT Cask Model in Horizontal (left) and Vertical (right) Plane

After setting up the physical model of the cask and fuel subassemblies, the isotropic angular photon source distribution and energy spectrum were determined. It was assumed that all photons were generated and uniformly distributed in the fuel regions of the discharged subassembly. The photon energy spectrum was calculated based on the activities of nuclides in the fuel region obtained from [17]. The depletion calculation was performed using the MCB code [18]. The activities of important nuclides after 20 years of operation are summarized in Table 4. The selected radionuclides were included in this analysis as per analyses completed previously in the HEU FSAR. The operation history is listed in Table 5. This operating history was derived from analyses completed previously in the HEU FSAR, where a similar operating history was used. This history assumes 20 years of weekly steady state operation at 4 hr (120 kW) and two executions of typical transients tests per week, with each transient producing 2500 MJ. Near the end of the 20 yr period, an aggressive testing program is assumed, where for the 33 days prior to the accident, a 3500 MJ transient is generated every 8 hrs. The final accident scenario is an overpower event that produces 6000 MJ. No decay time is assumed in the depletion calculation, which was also assumed in previous dose analyses completed in the HEU FSAR.

Table 4: Nuclide Activities Over All Burnable Zones in TREAT After 20 Years of Operation

Isotope	Activity (Ci)	Isotope	Activity (Ci)	Isotope	Activity (Ci)
Np239	2.95E+04	Cs137	2.03E+02	U236	1.22E-03
Ba140	6.06E+03	Kr85	3.25E+01	I129	1.57E-04
Pr143	5.48E+03	Sm151	5.55E+00	Rb87	1.16E-07
Ce141	3.93E+03	Pu239	1.35E+00	Sm147	2.73E-08
Y91	2.72E+03	Tc99	4.02E-02	Nd144	3.41E-12
Sr89	2.60E+03	U235	3.61E-02	Sm149	5.63E-13
Zr95	2.17E+03	U238	2.32E-02	Ce142	1.89E-13
Ce144	9.58E+02	Zr93	5.93E-03	Nd145	1.09E-13
Pm147	2.88E+02	Cs135	3.59E-03	Se82	4.72E-18
Sr90	2.57E+02	Sn126	2.71E-03		

Table 5: Power History of TREAT

Duration	Power (W)
30 days	1.11E+04
90 days	1.11E+04
240 days	1.11E+04
1 year	1.11E+04
3 years	1.11E+04
5 years	1.11E+04
5 years	1.11E+04
5 years	1.11E+04
7 days	0.00E+00
33 days	1.22E+05
10 sec.	6.00E+08

The photons emitted in different energy intervals from different isotopes were obtained from the ORIGEN2.2 photon library [19], which divides the photon yield into 12 to 18 energy groups depending on the isotope. Then, the overall photon energy spectrum was obtained by averaging all of the individual photon energy spectra over all isotopes weighted by their activities. The results are listed in Table 6.

The photon flux tallied in cells surrounding the cask was converted to dose rate in units of rem/hr/source using the ANS standard [20]. Then, the tallied dose rate was multiplied by the source strength (8.68E12 Bq) to obtain the real dose rate around the cask.

Table 6: Photon Energy Spectrum in the Fuel Region of a Discharged Fuel Subassembly

Average Group Energy (MeV)	Fractional Photon Yield
0.01	4.34E-01
0.025	3.09E-02
0.0375	2.23E-02
0.0575	1.95E-02
0.085	7.15E-02
0.125	2.23E-01
0.225	1.38E-01
0.375	2.00E-02
0.575	1.56E-02
0.85	2.53E-02
1.25	1.11E-04
1.75	1.67E-13
2.25	9.57E-14
2.75	5.49E-14
3.5	4.84E-14
5	2.04E-14
7	2.30E-15
9.5	2.61E-16

3.3.2 Results

The dose rates at different axial locations outside the cask are listed in Table 7 along with their statistical uncertainties. All uncertainties are less than 1% except for cell 1, where the relatively large, but negligible, error is due to low source impingement in this region. Based on 10 CFR § 20, the dose rate limit for an unlimited access area is 0.25 mrem/hr. Thus, the photon dose rate outside a TREAT cask is orders of magnitude smaller than the limit.

The photon flux distribution (p/cm^2/source) is presented in Figure 6. This shows that the region above the top of the cask (light green area and above) has a higher photon flux level than the flux level at the outer radius of the cask. However, the region above the cask is covered with heavy steel lifting equipment and is generally not a location where people handling the cask would be located (assuming personnel are not allowed on the crane bridge during fuel assembly transfer operations). Thus the dose rate is not calculated there.

Table 7: Photon Dose Rate Outside the Cask

Cell	Dose Rate (mrem/hr)	Error (%)
1	6.91E-07	0.59
2	5.80E-04	0.06
3	2.41E-03	0.03
4	2.50E-03	0.03
5	5.52E-04	0.06
6	2.72E-04	0.10

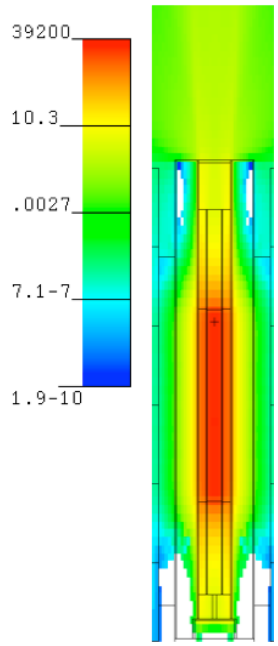

Figure 6: Photon Dose Rate Distribution Around a TREAT Cask

3.4 Photon Dose Rate Evaluation Above the Storage Area

The photon dose rate was evaluated above the spent fuel storage area. The radiation dose limit was obtained from two sources, and the more restrictive limit was utilized. In the United States Code of Federal Regulations (10 CFR § 20) [15] the annual occupational limit of the total effective dose equivalent is 5 rem. On the other hand, the ICRP [16] recommends the annual occupational dose to be 50 mSv (5 rem) and limits the dose received over a 5-year period to below 100 mSv (10 rem).

This analysis was completed using the Baseline 2.0 iteration of the LEU core design as a reference. This assessment is considered bounding for any core design that exhibits a lower or similar flux, with a similar photon spectrum. A description of similar analyses completed for the HEU core can be found in Sections 9.5.1 and 12.3.2.2 of the HEU FSAR.

3.4.1 Methodology

The Monte Carlo code MCNP6 [13] was employed to perform the shielding calculation. The weight window variance reduction technique was used to ensure the calculation could be completed in a reasonable time. The storage model is presented in Figure 7 in both horizontal and vertical planes. It was assumed that a discharged TREAT fuel assembly was stored in every storage hole, using the fuel assembly design summarized in Section 0.

The isotropic angular photon source distribution and energy spectrum for a single TREAT discharged fuel assembly were assumed to be the same as that described in Ref. [21]. It was assumed that all photons were generated and uniformly distributed in the fuel regions of the discharged fuel assembly. The emitted photon spectrum is listed in Table 8. The photon emission rate for a single discharged fuel assembly is 8.68E12 Bq. There are 147 storage holes, and therefore the total photon emission rate is 1.28E15 Bq assuming every storage hole is filled with a discharged TREAT fuel assembly. This value was used to normalize the results tallied in MCNP6. The dose rate was tallied in the region of 50 cm height above the storage holes.

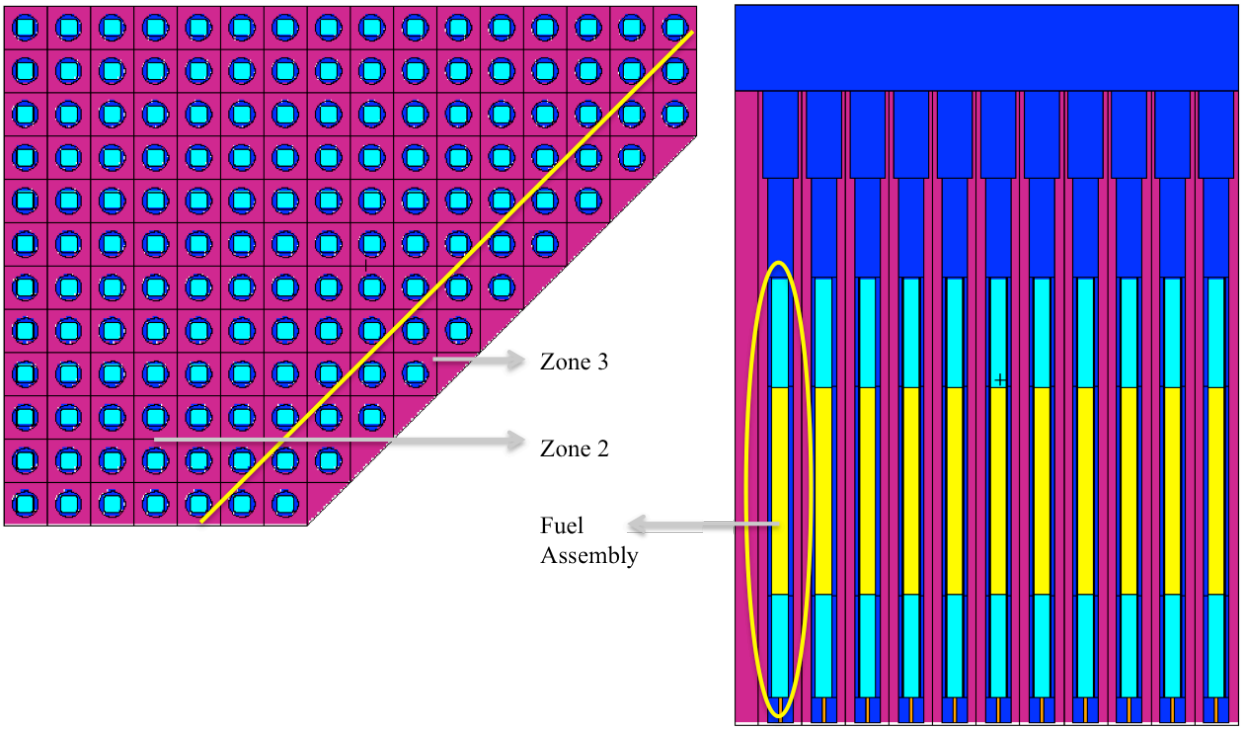

Figure 7: The MCNP6 Model of the Storage Area in Horizontal (left) and Vertical (right) Plane

Table 8: Photon Energy Spectrum in the Fuel Region of a Discharged Fuel Assembly

Average Group Energy (MeV)	Fractional Photon Yield
0.01	4.34E-01
0.025	3.09E-02
0.0375	2.23E-02
0.0575	1.95E-02
0.085	7.15E-02
0.125	2.23E-01
0.225	1.38E-01
0.375	2.00E-02
0.575	1.56E-02
0.85	2.53E-02
1.25	1.11E-04
1.75	1.67E-13
2.25	9.57E-14
2.75	5.49E-14
3.5	4.84E-14
5	2.04E-14
7	2.30E-15
9.5	2.61E-16

3.4.2 Results

A sensitivity study was performed to evaluate the average dose rate above the storage area with different thickness of steel plugs. The results are listed in Table 9. To satisfy the dose rate limit of 0.25 mrem/hr, a 7-8 cm thick steel plug is required above the storage hole filled with irradiated TREAT assemblies.

Table 9: Photon Dose Rate Above Storage Area

Plug Thickness (cm)	Dose Rate (mrem/hr)	Error (%)
0	6.45	2.37
10	7.45E-02	1.62
20	3.39E-03	2.31

3.5 Comparison of Neutron Fluxes at Detectors in M8CAL

This analysis was completed using the Variant 2.1 iteration of the LEU core design as a reference. This assessment is considered bounding for any core design that exhibits similar flux behavior. A description of relevant discussions for the HEU core can be found in Sections 3.1.2 (General Design Criteria 13), 7.2, and 7.7 of the HEU FSAR.

The purpose of this analysis was to compare the neutron flux reaching the power detectors located at the four corners of the concrete bioshield between the HEU and LEU (Variant 2.1) cores. The detectors' response to the neutron flux is a key parameter for the core conversion because the power coupling factor (PCF) is essentially representative of the ratio of TREAT neutrons leaking into the centrally-located test hole to those leaking into power meters at the edges of the core [22]. Figure 8 shows the location of the holes in which the power meters in the bioshield are located. All of the holes are horizontal and at the midheight of the core. The detectors are located at the hole ends closest to the core.

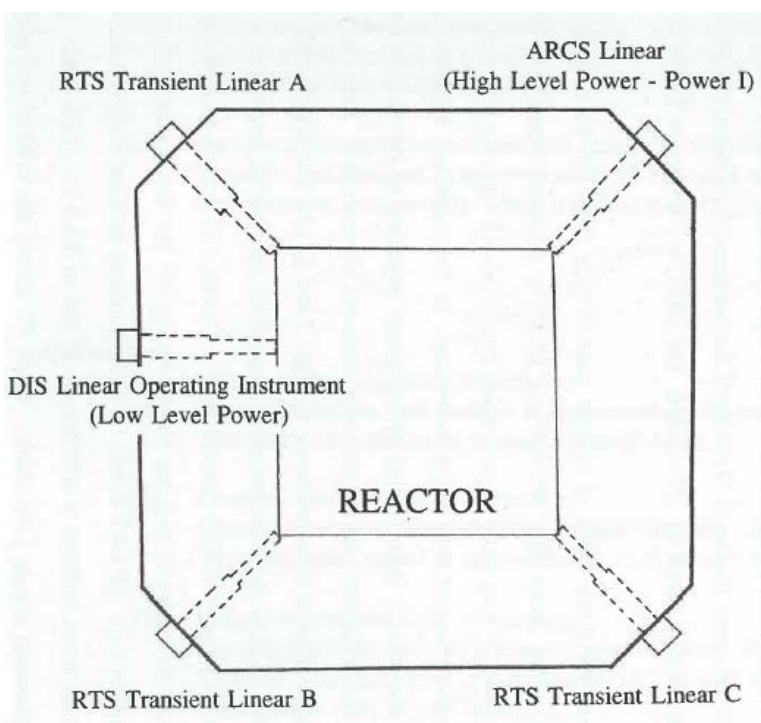

Figure 8: Configuration of the Instrumentation in the TREAT Core

3.5.1 MCNP Calculations

The responses of the I, A, B and C detectors (used during transient irradiations) were calculated with MCNP5 with an F4 tally to get the total neutron flux, as well as the thermal neutron flux with an energy bin set with a highest energy of 0.625eV. The instruments and the electronics were not simulated in MCNP, and the neutron flux was tallied inside the cylindrical holes that were modeled as being filled with dry air. The statistical uncertainty of the tally calculation was 1.2%. The flux is assumed to be generated from an isotropic angular source.

The rod configuration used in the calculations was with the control/shutdown rod partially inserted and the transient rods 100% withdrawn. This configuration reflects the end of a temperature-limited transient. (In actual practice, burst-type transients are started with the core at critical state (with control/shutdown and transient rods partially inserted), and then the transient rods are withdrawn at maximum speed, which is fast enough that the core power hardly changes before the rods are fully out.) The MCNP calculations were performed using the cross section libraries set at 'room' temperature (293K). Table 10 shows the ratio of the thermal and total neutron flux of the LEU to the HEU core. It should be noted that the tally results were divided by the resulting k_{eff} assuming that both core are at critical state.

Table 10: LEU/HEU Ratio of the Thermal and Total Neutron Flux Reaching the Detectors' Location

	LEU/HEU Ratio	
Instrument Name/Location	**Thermal Neutron Flux (<0.625eV)**	**Total Neutron Flux**
Power-I [North-East]	91%	90%
Power-A [North-West]	87%	88%
Power-B [South-West]	91%	92%
Power-C [South-East]	90%	89%

Due to the neutron spectrum hardening in the Variant 2.1 LEU core, the thermal and the total flux are both less by approximately 10% based on the assumption that the two cores are being operated at the same power level. However, considering the anticipated increase in core power required from the LEU core (for Variant 2.1) in order to achieve the same test sample energy depositions as the HEU core (for example, in the case of the M8CAL fuel pin irradiation, the LEU core was estimated to need 26% higher power [4]), it is expected that the neutron fluxes at the detectors in the case of the LEU core will be higher than in the HEU core.

The radial reflector surrounding the core is 2ft thick, so the neutrons reaching the detectors are well-thermalized. Thus, the ratio of the thermal to the total neutron flux are at the same level for the HEU and the LEU cores, as shown in Table 11.

Table 11: Thermal to Total Neutron Flux Calculated with MCNP for the HEU and the LEU Cores

	Thermal to Total Neutron Flux Ratio	
Instrument Name/Location	**HEU**	**LEU**
Power-I [North-East]	92%	92%
Power-A [North-West]	93%	91%
Power-B [South-West]	93%	92%
Power-C [South-East]	95%	95%

3.5.2 Conclusion

The neutron flux reaching the power detectors was calculated with MCNP for the M8CAL half-slotted core loading and assuming LEU fuel assembly design Variant 2.1. At the same core power, there is a 10% decrease in the thermal and the total neutron fluxes in the Variant 2.1 LEU core as compared to the HEU, as shown in Table 10. The increased clad thickness and larger fuel-clad gap cause increased absorption

and axial leakage, respectively, and therefore reduce the flux reaching the detectors. The decrease in relative flux is expected to be compensated for by the higher core power the LEU is expected to produce to achieve equal sample energy depositions with the HEU core, for designs such as Variant 2.1 which have a reduced PCF compared to the HEU core. The analyses will be extended to study the neutron fluxes at the detectors as the core heats up (leading to the increase in neutron leakage as the neutron spectrum is hardened) and compare the results for the HEU and the LEU cores. A study on the impact of core temperature on detector response has been performed for the HEU core [4] [23] [24], and will be evaluated for LEU once the design is more finalized.

4. Thermal Hydraulic Analyses

This section discusses the ancillary thermal hydraulic analyses completed in support of TREAT conversion efforts. Additional thermal hydraulic evaluation of the different LEU design concepts can be found in [4] and [23]. These analyses are largely focused on ensuring that temperature-derived safety limits are not violated and that all principal support systems for core safety can continue to function as intended at the temperatures it is expected they will experience. For all analyses presented here, methodologies are utilized that are consistent with, or improved from, those used in the HEU FSAR. Results calculated for the LEU core are compared to historical data obtained from HEU TREAT operation, when the data is available.

Ancillary analyses discussed in this section include a qualitative discussion of heat transfer from the test vehicle to neighboring fuel assemblies (Section 4.1), heating in the permanent reflector and grid plate (Section 4.2), and thermally-induced distortion of the grid plate (Section 4.3). While all of the analyses in this section are considered to be complete and have been reviewed for technical content, it should be noted that all topics will be revisited once the LEU design has achieved a final stage of maturity. In most cases, it is expected that the analyses presented here will act as bounding analyses, but additional calculations will be performed where the margin to satisfy the various safety criteria is not sufficiently large.

4.1 Heat Transfer From Test Vehicle to Core

Due to the need to limit TREAT fuel assembly peak temperatures, the potential for heat transfer from in-core experiment hardware ("vehicles") to adjacent TREAT fuel assemblies must be considered. Test fuel contained in in-core vehicles can reach high temperatures. In many experiments, the test fuel is heated beyond its melting temperature and, in some experiments, even to its vaporization temperature. Much of that heat is subsequently transferred to components within the vehicle. Other sources of heating of the test vehicle may also be present, such as electrical heaters. If the heat is transferred to the vehicle's exterior surfaces such that it causes those surfaces to become hotter than the facing surfaces of adjacent TREAT fuel assemblies, some heat could be transferred to those assemblies. Of course, the TREAT fuel assemblies will already be hot due to the core power generated during the transient. Depending on the individual experiment, there is the potential for heat transfer from the experiment vehicle to the adjacent fuel assembly causing unacceptably high assembly temperatures. The TREAT facility historical "Guide for Irradiation Experiments in TREAT" required this topic to be addressed in experiment safety analysis reports. The following discusses the complexities involved in such an evaluation and an approach that was used historically.

Regarding heating within TREAT fuel assemblies, during typical transients, heat is generated in the fuel nearly adiabatically, with little time for heat transfer from fuel to cladding. Thus, the cladding begins to be heated after most of the transient energy has been generated. The temperature of the cladding of any TREAT fuel assembly as it absorbs heat from the fuel depends on several factors: the total amount of fission energy that was generated by the fuel, the masses and heat capacities of the fuel and cladding, the heat transfer coefficient between the fuel and cladding, the axial heat conduction from the fuel to the ex-core regions of the fuel assembly, and heat loss from cladding to coolant. The heat transfer thus depends upon the particular design of the fuel assembly.

Regarding heating of the test fuel, according to the TREAT Guide, the amount of heat generated in the test fuel during an accident transient must take account of test-fuel relocation occurring during the power

transient and the changing power coupling between core and test fuel that is due to the changing test-fuel configuration. How the configuration changes depends on the design of the test-vehicle. The change might be due to melting of the fuel or by some components of the vehicle becoming damaged (e.g., fractured or melted) by the heat generated by the test fuel, or by chemical or mechanical interaction with the test fuel. Conservative scenarios must be assumed. If the assumed movement of the test fuel involves dispersal and a decrease in fuel self-shielding from the neutron flux, there may be an increase in the fuel power coupling factor. Furthermore, the heat existing in the test vehicle itself at the start of the transient must be taken into account when calculating the total test-vehicle heat existing at the end of the transient.

The way heat generated within the test fuel is transferred to the vehicle's exterior surface also depends upon the particular design of the vehicle. Vehicles are typically designed to protect the primary containment wall of the vehicle from being overheated to the extent that it would not maintain containment integrity during and after the transient. Protection is usually provided by intervening materials having significant heat capacity and mass or having low thermal conductivity. Furthermore, if the test vehicle needs to be hot at the start of the transient, there will probably be insulation around the exterior of the primary containment. This may be enclosed by a secondary containment (or confinement), which has been historically required whenever the test fuel has been pre-irradiated or contains plutonium. These components further restrict heat transfer to the vehicle's outer surface. Vehicle designs, quantity of test fuel, power coupling between test fuel and reactor, and reactor energy and core reactivity needed for the experiment are all experiment-specific, resulting in the need for experiment-specific safety analyses.

The complexity involved in a detailed heat-transfer analysis from test vehicle to the cladding of adjacent reactor fuel assemblies (simultaneously with fission-heat transfer from the assembly's fuel to its own cladding) was avoided in practice by addressing simplified, but conservative, scenarios. In many of the more-recent TREAT tests performed prior to 1994, particularly those involving complex experiment vehicles and large quantities of test fuel, the simplifying assumption was that the test vehicle and several TREAT fuel assemblies immediately adjacent to the vehicle come into thermal equilibrium with one another after the power transient, with no heat loss to other components. The slowness of heat transfer from test fuel to the vehicle outer surface, the slow heat transfer from the reactor fuel to the assembly cladding, and the assumed absence of any coolant air flow after the accident, justifies this equilibrium approach.

Generally the hottest core assemblies are not so close to the core center as to be adjacent to a test vehicle in the core center. Thus, the heat generated by the (cooler) fuel assemblies adjacent to the test vehicle can be expressed in terms of the total energy generated by the core times the fraction (F) of the total core energy that was generated by those adjacent assemblies. The value of F depends upon several factors including the fuel assembly design (the fuel's C/U ratio, density, and volume), the number and locations of assemblies in the core, and the axial positions of the control and transient rods during the power transient. One conservative assumption often made was that the assemblies immediately adjacent to the test vehicle were also the assemblies that generated the most energy in the core (the ones with the highest self-heating).

TREAT operations involve multiple features that will prevent reactivity accidents resulting in fuel assembly cladding temperatures from exceeding their safety limit if the only heat source is the assembly's own fuel. Heat will not transfer to that assembly from test-vehicle outer surfaces having a lower temperature than the TREAT fuel assembly. (Instead, heat would transfer from the TREAT fuel assembly to the vehicle.) Thus, the safety evaluation becomes additionally simplified if the equilibrium temperature

of the test vehicle, without considering any heat loss from the vehicle, is less than the maximum-allowable cladding temperature of TREAT fuel assemblies. On the other hand, if the test vehicle, without external heat loss, has an equilibrium temperature greater than the maximum-allowable cladding temperature of a TREAT fuel assembly, then a potential for overheating the TREAT assembly cladding would be possible. The issue then becomes: is this more likely to happen in the LEU core than in the HEU core for a maximum experiment allowable in the HEU core?

The potential for such heat transfer in an LEU-fueled core compared to that in an HEU-fueled core will depend on (a) how the core temperatures due to self-heating will vary between the two cores and (b) how the vehicle temperatures due to heat sources within the vehicle will differ during the reactivity accident for an experiment in an LEU core compared to the reactivity accident for the same experiment in the HEU core. The power-time histories in the two accident transients will be different due to different neutronic characteristics of the two cores. (The core's neutronic parameters of importance are the core loading for the experiment, the reactivity feedback, the prompt generation lifetime, the delayed neutron fraction, the axial power profile, the masses and heat capacities of the fuel assembly fuel and cladding, the starting positions of the control and transient rods, and the local flux depression due to the presence of the test vehicle.) The extent to which the accident transients differ between the two cores also depends upon the amount of reactivity needed in each core to perform the experiment transient. The LEU vs. HEU comparison will also depend upon the maximum-allowable temperature set for the cladding of the LEU fuel assemblies.

This analysis will be performed after the LEU fuel assembly design concept has been established. The analysis will probably be based on a case which (a) assumes that the hottest fuel assembly in the LEU core will result in higher cladding temperatures than the hottest fuel assembly in the HEU core, for core reactivity accidents corresponding to the same planned experiment test-fuel power and energy generation and (b) considers an experiment that was actually performed in the HEU core and that generated exceptionally-high accident energies (core energy and test-fuel energy) as well as high post-transient vehicle equilibrium temperatures. An experiment that meets the latter criteria is the LO4 test. It employed seven high-fissile-content fuel pins with a fuel height of approximately one meter and utilized a Mark-IIIC sodium loop. The power transient in the experiment generated approximately 2000 MJ of TREAT energy. The amount of test fuel energy that was generated during the experiment, and the amount of energy that would have been generated if there had been a maximum reactivity accident, were both apparently the highest of any experiment that was performed in TREAT. This test will provide a reasonable empirical basis for determining a corresponding maximum-permissible test in the LEU core. That limiting test would then be the reference for comparing the impact of such a test on heating of the LEU core versus on HEU core.

4.2 Thermal Hydraulic Analysis of the Permanent Reflector and Core Support

The following thermal-hydraulic analysis focuses on heating of the permanent (radial) reflector and core support (grid-plate) during constant-power operation (120 kW) as well as during a reactivity accident scenario. The temperature distribution of the grid plate supports the structural analysis calculations of a) the core support in the event of an earthquake and b) the maximum-allowable thermal expansion of the plate as to prevent excessive bowing of the control-rod thimbles and hinder the movement of the control rods. For all analyses conducted, the half-slotted core loading of the M8 power calibration experiment (M8CAL) is used [4] [25]. Both HEU and LEU (Variant 2.1) fuel element assemblies were evaluated for comparison [4]. It is also assumed that the reactor is always convectively cooled by air at flow rates up to the nominal 6000 cfm. The assumption of forced-convection air flow is conservative in the grid-plate

analysis in that it results in faster heat transfer from the core to the grid plate, consistent with the assumption of no heat transfer from the grid plate to the concrete that supports the grid plate.

This analysis was completed using the Variant 2.1 iteration of the LEU core design as a reference. This assessment is considered bounding for any core design that is expected to produce peak fuel temperatures below those produced for the variant referenced in this particular analysis. A description of similar analyses completed and discussions of this topic for the HEU core can be found in Sections 4.3.2.2, 4.3.6, 15.3.2.3, and 15.9 of the HEU FSAR.

4.2.1 Geometrical Domain

The components of TREAT that are relevant to this study are the core lattice (core), permanent (radial) reflector, and core support plate (grid-plate). Figure 9 below illustrates the TREAT reactor facility [6].

Core

The core consist of approximately 4-inch x 4-inch square fuel assemblies with chamfered corners. The upper and lower sections of the assembly contain 2-ft graphite axial graphite reflectors, and the central 4-ft-long section contains the fuel (HEU or LEU dispersed in graphite). The fuel assemblies are cladded entirely with zircaloy in the case of LEU fuel or by both zircaloy (on the fuel region) and aluminum (on the reflector region) for the HEU fuel [5]. The fuel is in direct contact with the axial reflectors for the LEU design. However, for the HEU design the fuel is separated by a ¼" very-low-conductivity gap above and below the fuel blocks. The intent of the gap is to delay heat transfer from the fuel to the reflector sections and therefore protect the aluminum cladding from overheating. In addition to the standard fuel assemblies, the core also includes other special-purpose elements such as control rod fuel elements each with a 2-inch-diameter longitudinal control-rod hole. Figure A - 1 in the Appendix shows the core configuration for the M8CAL experiment that was used in this analysis in more detail [4] [25].

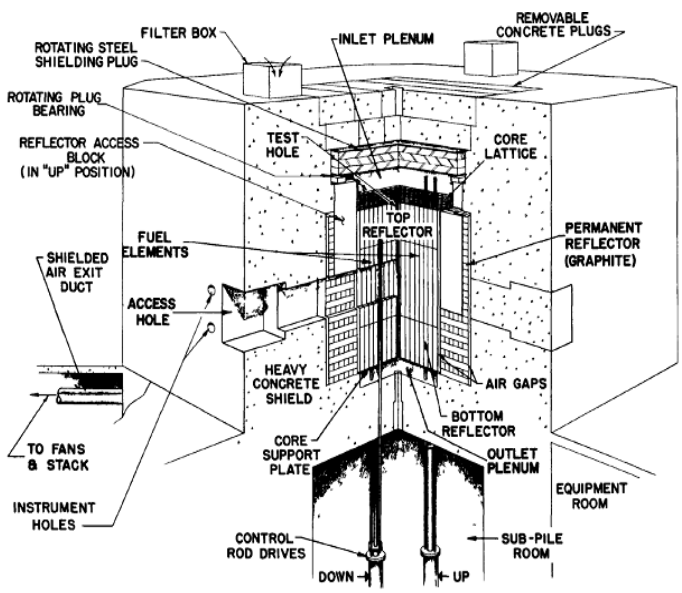

Figure 9: Perspective View of TREAT [6]

The core is cooled with air forced axially downward through engineered channels between the assemblies [23], with the flow rate controlled by two 40-hp turbo-compressors operating in parallel. Each turbo-

compressor is rated at 3250 cfm [5]. The air exits from the plenum chamber below the core through two ~10 in. diameter ducts leading to the exhaust filtration system in the turbo-compressor room. All flow can be caused to pass through the core (and permanent reflectors), or part of it (up to 3000 cfm) can be caused to by-pass the core by flowing instead through the subpile room below the core. Utilization of bypass flow is intended to cool the reactor effluent air downstream of the core and ensure that the air is below the temperature limit of the filtration/cooling system (~200 °C).

Permanent radial reflector

The core is radially surrounded by a permanent radial reflector consisting of graphite blocks (4-inch x 4-inch), stacked 7 ft 8in. high and 2ft thick along the four inside walls of the shield cavity. There is a nominal 2-in. gap on the inner and outer faces of the reflector providing for cooling flow. The permanent reflector is supported by angle iron spacers and a sheet metal framework anchored to the steel liner of the concrete shield cavity that surrounds the reflector. There is a gap formed by the spacers and support bars, which allows for the passage of coolant flow between the reflector and the concrete. The permanent reflector graphite is enclosed (but not sealed) within the liner.

Grid plate

The total weight of the core components is supported on a low-carbon steel (A36) grid plate, 6 ft 7 in. square and 1 in. thick. Figure 10 shows a top view of the grid plate [5]. Several openings in the grid plate are machined as to accommodate air cooling passages, pathways for control rods, as well as fuel positioning openings to provide fuel assembly alignment.

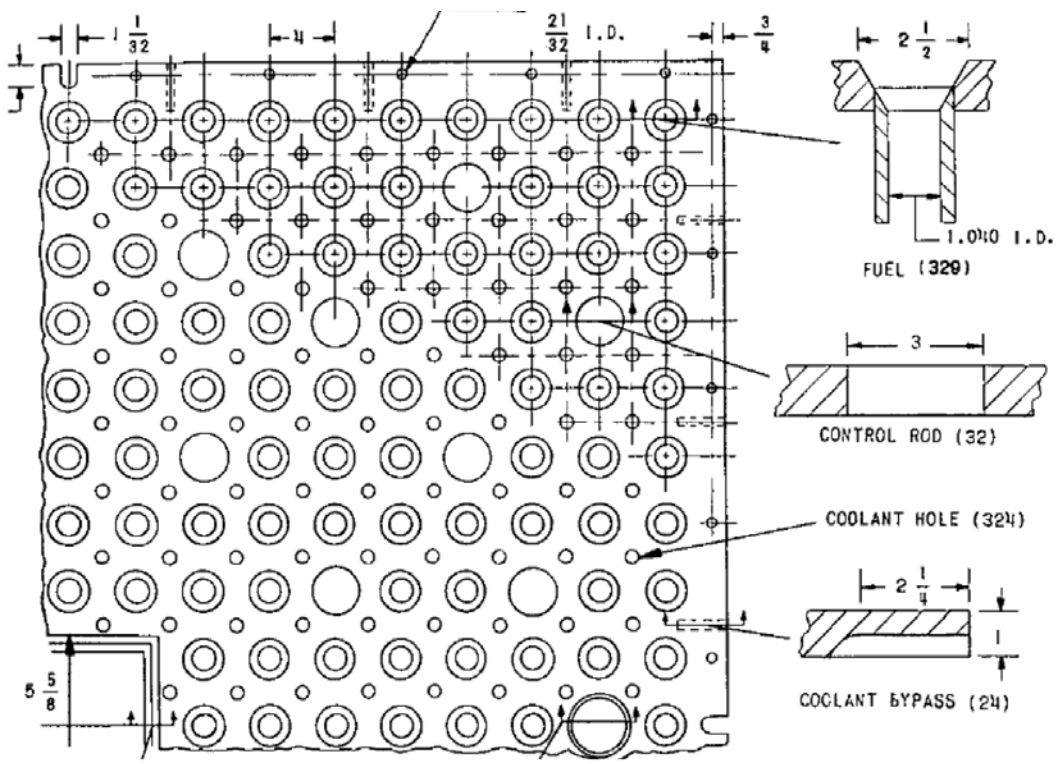

Figure 10: Drawing of a Quarter Section of the Core Grid Support Plate [5]

The fuel alignment openings (1.040 in. ID) are countersunk to assist the leading of the guide pin at the bottom of the fuel assembly. There are a total of 329 fuel alignment openings, but control-rod openings (3 in. ID) can also be adapted and used as fuel positions if desired. A total of 324 (7/8 in.) flow openings are provided in the plate, aligned with the coolant passages formed at the chamfered corners of neighboring assemblies. Approximately 10% of the flow is distributed equally in the flow passages between the radial reflector and core/bio-shield [26]. This is accomplished by 24 coolant bypass slots (0.5x0.5x2.25 in) spaced uniformly below the edges of the plate. The edges of the plate are supported on the concrete ledge, which forms the coolant plenum chamber, and the central area of the plate is supported by the control-rod thimbles. The plate is not fixed to the thimbles, however, and thus the plate is free to thermally expand [5].

4.2.2 Model and Methodology

The ancillary thermal-hydraulic analysis of the radial reflector and grid-plate ideally would be the outcome of an integrated core model. Such a core model, even a simplified one, would be too complex to develop in support of this limited analysis. Rather, some conservative assumptions in the grid plate and reflector analysis would suffice and would allow for a relative comparison between HEU and LEU cores. At this point, the grid plate and radial reflector thermal analysis will be decoupled from a core model. However, in order to properly analyze the heating of the grid plate, it is necessary to determine the heating due to conduction from supported assemblies as well as convection from the air exiting the core and radial reflector, respectively. This is done using temperature boundary conditions as a function of time for the grid plate, as described below.

Let us consider a planar geometry, as shown below in Figure 11, for the geometrical domain of interest. Here we define three regions, denoted as R_i, to establish the gas-phase temperature exiting the core and permanent reflector.

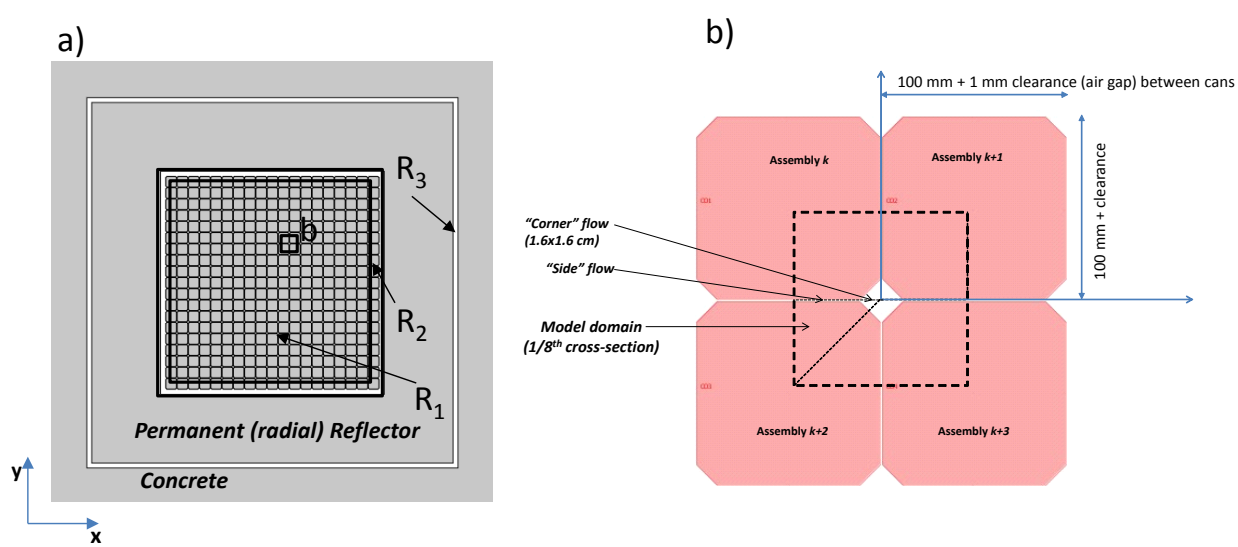

Figure 11: a) Schematic Cross-Section of TREAT, b) Four neighboring fuel assemblies form a cooling passage

Region 1 (R_1)

Approximately 90% of the total air flow enters in R_1, where the flow is assumed to be distributed equally among the assemblies. The majority of that flow, approximately 97%, is in turn distributed to coolant passages formed at the chamfered corners of neighboring assemblies, Figure 11b [4]. The gas-phase temperature as a function of time was calculated for each flow passage based on LEU/HEU core power distribution; see Appendix A, Figure A - 2. To simplify the calculations, the temperature of the coolant air flow through the flow channels is calculated based on an average power between four neighboring assemblies. Assuming negligible heat transfer between neighboring fuel assemblies, symmetry is utilized for the geometrical domain (a 1/8th section is used, Figure 11b). Additional details on the assumptions utilized in the thermal hydraulic model of a fuel assembly can be found in [26].

Region 2 and 3 (R_2 and R_3)

Consider a planar region (Figure 12 below) between the fuel assemblies facing the radial reflector (R_2) that extends to the wall of the concrete in R_3. Heat is transferred from the assemblies to the radial reflector by thermal radiation and forced convection in region R_2. Heat is transferred in the reflector through thermal conduction (axially and radially), with cooling supplied by forced convection in region R_3. The air flow in R_2 and R_3 is mixed and exits through the radial slots of the grid plate at an average temperature of T_{mix}. The assemblies facing the radial reflector are assumed to be isolated from the rest of the core since neighboring assemblies have similar power distribution thus reducing lateral conductive heat transfer.

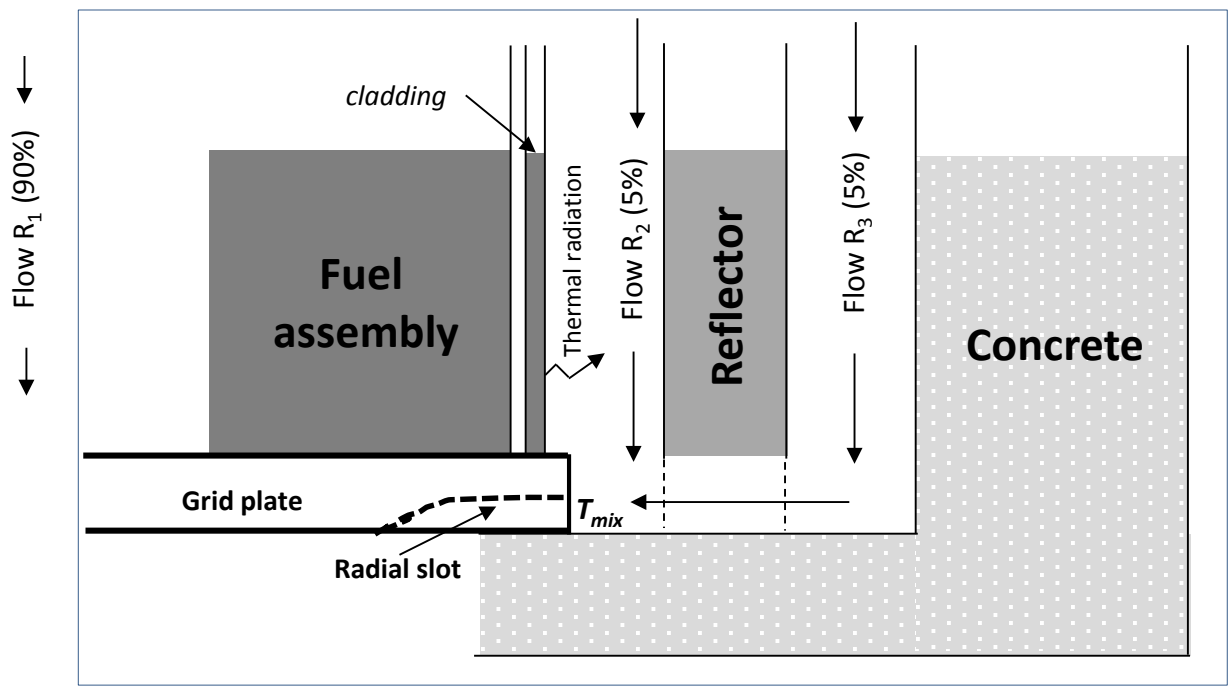

Figure 12: Schematic of Permanent Reflector and Flow Regions

The heat conduction in the permanent reflector in the lateral direction (through-plane in Figure 12) is neglected, and the model for region R_2 and R_3 is hence reduced to a 2D approximation. The flow regime in the respective region is laminar, even at the nominal air flow rate (6000 cfm) through the core. The

flow entering the permanent reflector is assumed fully developed. The thermal hydraulic model was solved using Comsol ® V3.5.

Grid plate model

A 3D model of the grid-plate according to the dimensions as given in Figure 10 was developed in Comsol®. Figure 13 shows the grid- plate configuration for the M8CAL core loading (20 transient rods). To reduce computational time, a solution is found for only a quarter of the grid plate (section Q2), with symmetry being assumed at the boundaries adjacent to other sections.

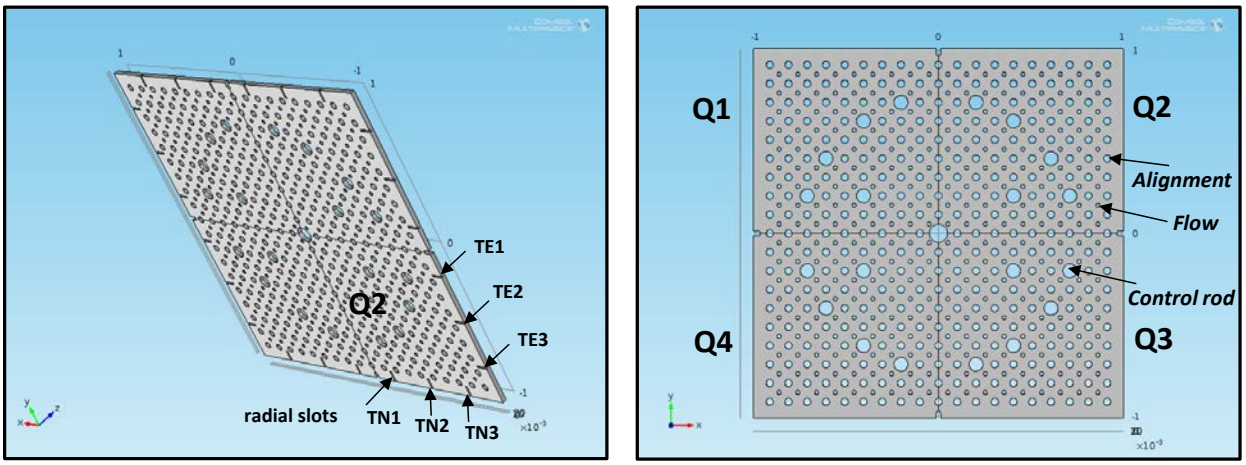

Figure 13: Grid Plate Configuration for M8CAL (without Fuel Alignment Pins)

Denoted in Figure 13 are openings in the plate for the alignment of the assemblies, flow holes, control rods, and the radial slots (TN_i and TE_i) on the north and east sides of the plate, respectively. The plate model considers heat conduction laterally and axially. Heat transfer by convection through the perimeter of the flow holes and radial slots is treated as a boundary condition. For each flow channel the gas-phase temperature as a function of time is calculated with a 3D model, described previously, and saved as a look-up table. Knowing the gas-phase temperature entering the flow holes during the transient (via the look-up table), the heat transfer rate to the plate is calculated using established heat-transfer correlations [23]. The same methodology is applied to the radial slots, in this case adopting the 2D model schematically shown in Figure 12. The temperature resulting from the mixing of air in R_2 and R_3, T_{mix}, as a function of time was calculated in discrete steps based on the number of fuel assemblies facing the permanent reflector. An average temperature from the discrete regions in the vicinity of each slot was then calculated assuming that the flow is distributed equally among all radial slots.

In addition to convective flow, the grid plate is also heated by axial heat conduction through the assemblies supported by the plate. A more detailed view of a grid plate section is shown below in Figure 14. Panel A shows the fuel alignment hole (with flow holes at each corner), and panel B shows the fuel alignment pin. Panel C shows the fuel pin resting on the grid plate section, and while not included in the figure, also the 9-ft-long fuel assembly which is welded together with the fuel alignment pin.

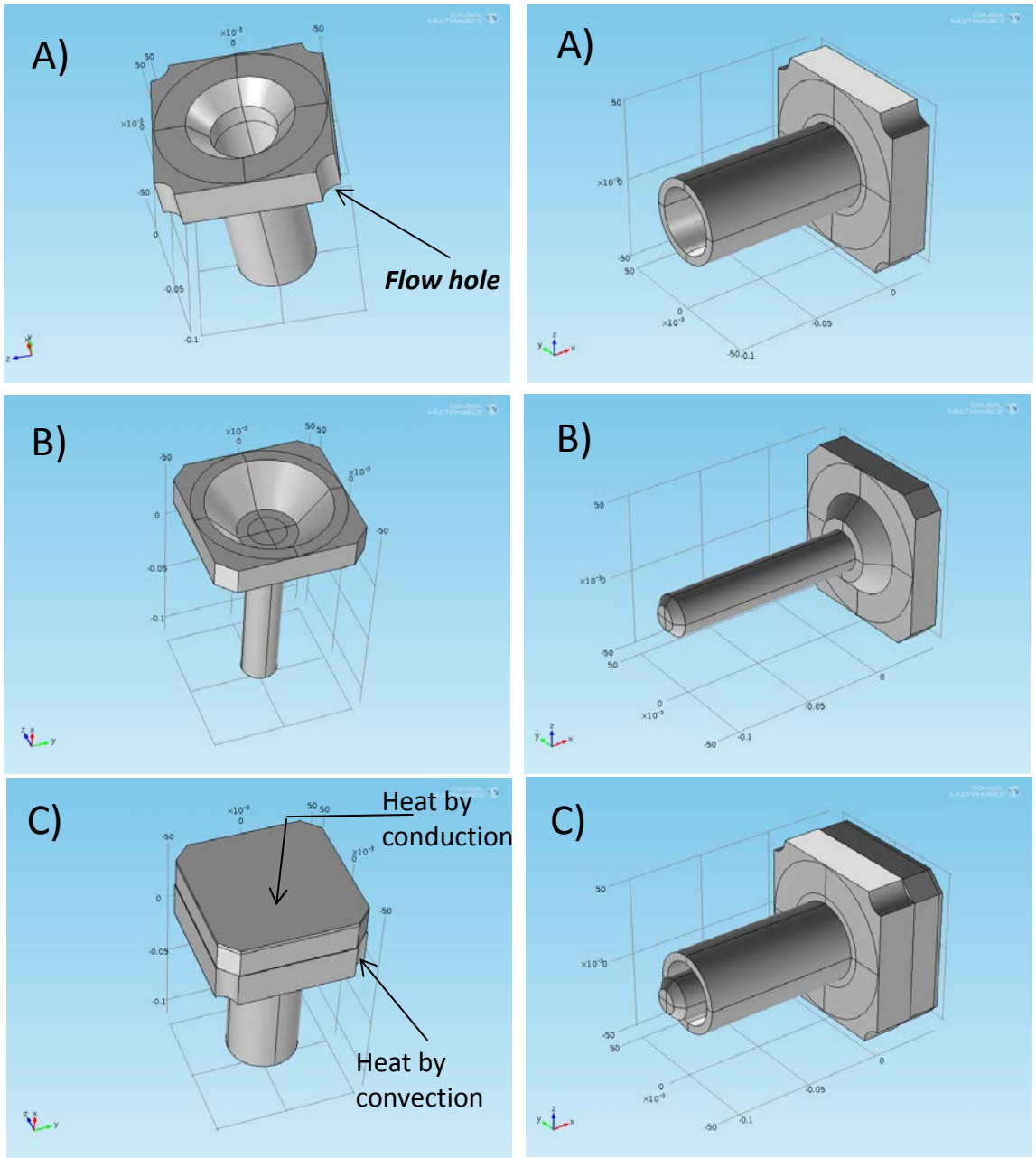

Figure 14: Section of the Grid Plate Showing: A) Fuel alignment hole, B) Fuel alignment pin, C) Fuel alignment pin attached to grid plate section

Since the fuel assembly is decoupled from the grid plate, heat by conduction is modeled as an imposed temperature at the top boundary of the alignment pin (see Panel C). The time-temperature history, T(t), was evaluated from the lower axial reflector which was calculated with the fuel assembly model [23].

4.2.3 Scope of analysis

With regard to accident analyses, the thermal analysis for the grid plate and reflector utilizes a MCNP-calculated core relative power distribution (see Appendix A) and power time history [4] derived for the bounding reactivity accident identified in the HEU FSAR as the design basis accident (DBA) in TREAT. The reactivity accident associated with this bounding case assumes that all of the reactivity available at

the beginning of the planned bounding shaped transient is inserted as a step [4]. The maximum-allowed reactivity had been determined during the M8CAL core operations as 5.95%. For the M8CAL test pins, there is a 26% decrease in the PCF[1] in the assumed Variant 2.1 LEU core compared to the HEU core. This means that an increase in core power for the LEU core is needed in order to achieve the same total energy deposition (TED) in a given test sample as the HEU core achieved. The 5.95% reactivity step insertion produced a total energy of 4.06 GJ for the HEU core compared to 5.59 GJ for the LEU. The corresponding peak fuel temperature of the hottest fuel assemblies were close to 820 °C for the HEU and ~960 °C for the LEU.

4.2.4 Results

Reflector

Oxidation of graphite is possible in the event the reactor becomes severely overheated. At temperatures below 300 °C[2], oxidation rates are small, however [5]. Given the large thermal mass of the permanent reflector, it is anticipated that the reflector will not be heated to such high temperatures. As noted in the Appendix A, when considering the accident case for the assumed LEU core design with a total core energy of ~5.6 GJ the temperature of the reflector remained below 60 °C. For comparison, the reflector remained ~ 10 °C cooler in the case of the HEU core. Figure 15 below shows the peak temperature of the permanent reflector as a function of time. Furthermore, the corresponding temperature of the neighboring fuel assembly and flow passage between reflector and core is shown at the time the permanent reflector reaches the highest temperature (~400 min).

[1] The relationship between TREAT core energy and energy in a test sample is expressed in terms of the PCF, as Joules per gram of test fuel per MJ of TREAT core energy.
[2] At 300 °C, graphite is oxidized at a rate of 2e-5 wt-%/hr [5].

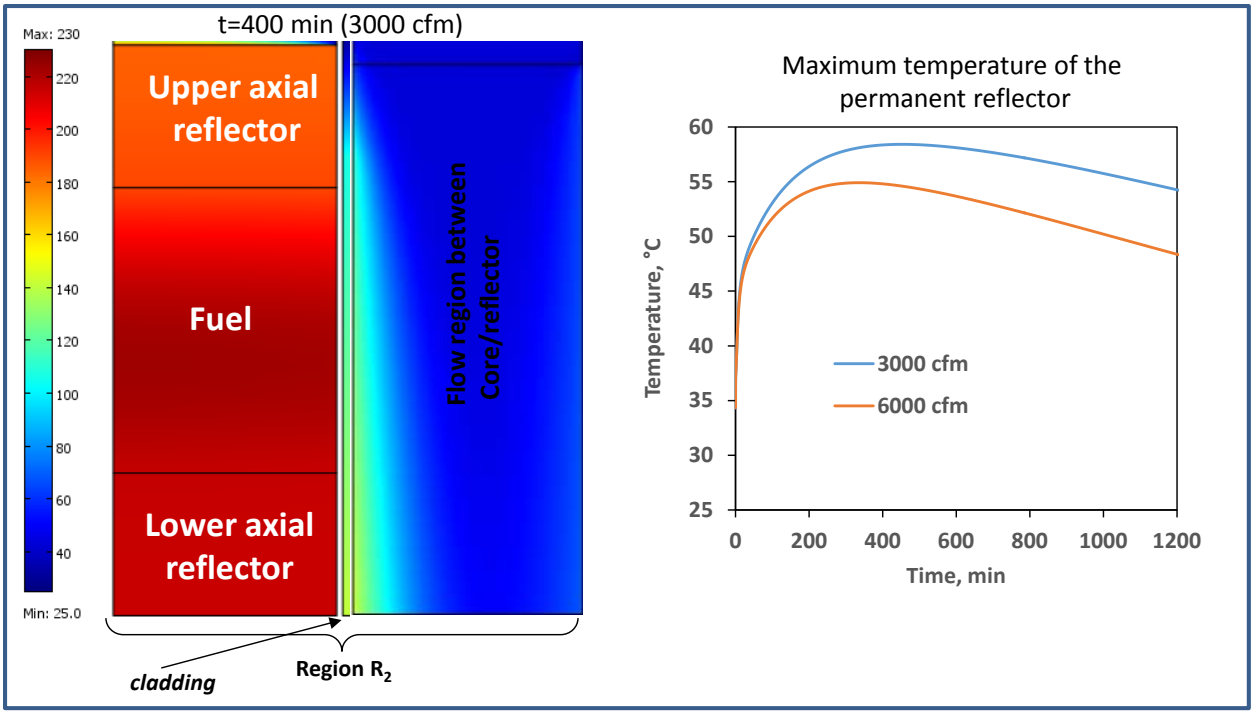

Figure 15: Maximum Peak Temperature History of the Permanent Reflector for the LEU Core as a Function of Cooling Rate

This case was calculated for the hottest fuel assembly at the inner periphery of the radial reflector. Approximately 20 MJ of energy was deposited in that assembly. All the energy is not transferred to the reflector because a fraction of the energy exits with the flow. Furthermore, the reflector is being cooled by air in the flow region between the reflector and concrete (bio-shield). The temperature near the bioshield remained close to the ambient temperature even when one turbo-compressor was used for cooling (assuming it operates at the nominal capacity of 3000 cfm).

Components of the TREAT facility not included this analysis are a 1/16-in thick aluminum sheet covering the core-face and top edge of the reflector, and a ¼-in thick steel liner (located 2 in. away from the reflector) that separates the outer periphery of the reflector from the concrete shield. It is anticipated that the reflector would be cooler when taking into consideration for the aluminum liner, as the liner would act as a thermal radiation shield.

In the absence of cooling, the energy that can be absorbed by the core and permanent reflector in this case would result in a temperature of ~160 °C[3] (thermal equilibrium). Severe oxidation of the permanent reflector (if any during normal core operation) is highly unlikely. However, it should be noted that the reflector is heated only from the heat transferred thermally from the adjacent fuel elements. The energy deposition in the permanent reflector from neutrons and photons was not included in this analysis and is subject to consideration in future work.

[3] Accounting only for the thermal mass of the core components (fuel, graphite and cladding) and radial reflector. Taking into consideration the thermal mass of the concrete surrounding the core, the equilibrium temperature would be substantially lower.

Grid plate

The maximum grid-plate temperature profiles (Q2) during the accident scenario for both HEU and Variant 2.1 LEU cores are shown below in Figure 16, for a coolant flow rate of 3000 cfm through the core.

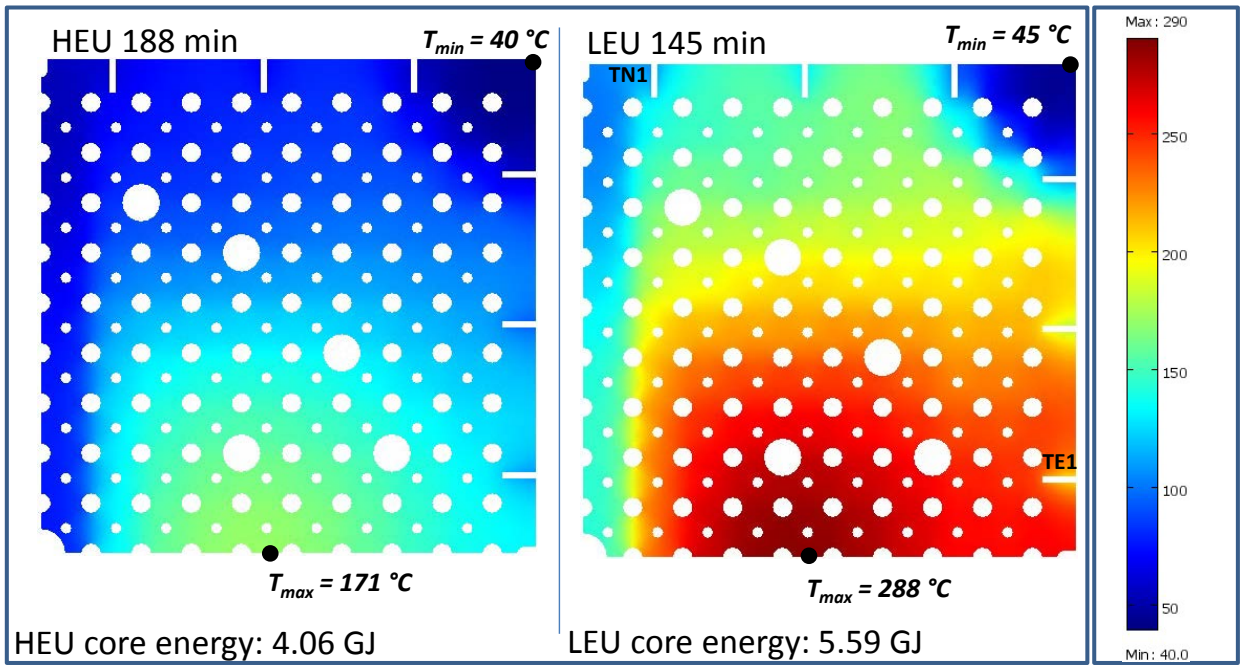

Figure 16: Maximum Grid Plate Temperature Profiles During a Reactivity Accident Scenario

The LEU grid plate reaches ~290 °C compared to 170 °C for the HEU core. With 6000 cfm of coolant flow, the maximum temperature was reduced by almost 50 °C. The respective grid plate temperatures are caused by differences between the designs of the HEU and LEU fuel assemblies. First, in order to achieve the same TED as the HEU core in a given test sample, the LEU core energy is higher. Second, more heat is conducted axially in the LEU fuel assemblies, since the fuel and axial reflectors are in contact. In case of the HEU design, axial conduction is impeded due to the ¼-in evacuated gap between the fuel and axial reflectors.

As the hottest fuel assemblies are located at the center of the grid-plate, the central part of the grid plate reaches much higher temperatures than the outer peripheral region for both cores. The upper right corner of the plate quadrant remains below 50 °C, as this region contains fuel elements filled only with graphite and used to provide additional reflector thickness. The time to reach the grid plate peak temperature coincides with the maximum temperature reached by the lower axial reflector and the fuel alignment pin.

Figure 17 shows the time-temperature histories for the LEU core for a) gas-phase temperatures at the exit of the cooling channels within the core, b) the temperature at the upper part of the alignment pins, and c) gas-phase temperatures entering the radial slots of the grid plate. In the figure, P denotes the average energy deposited in four neighboring fuel elements expressed as the percent of the total core energy.

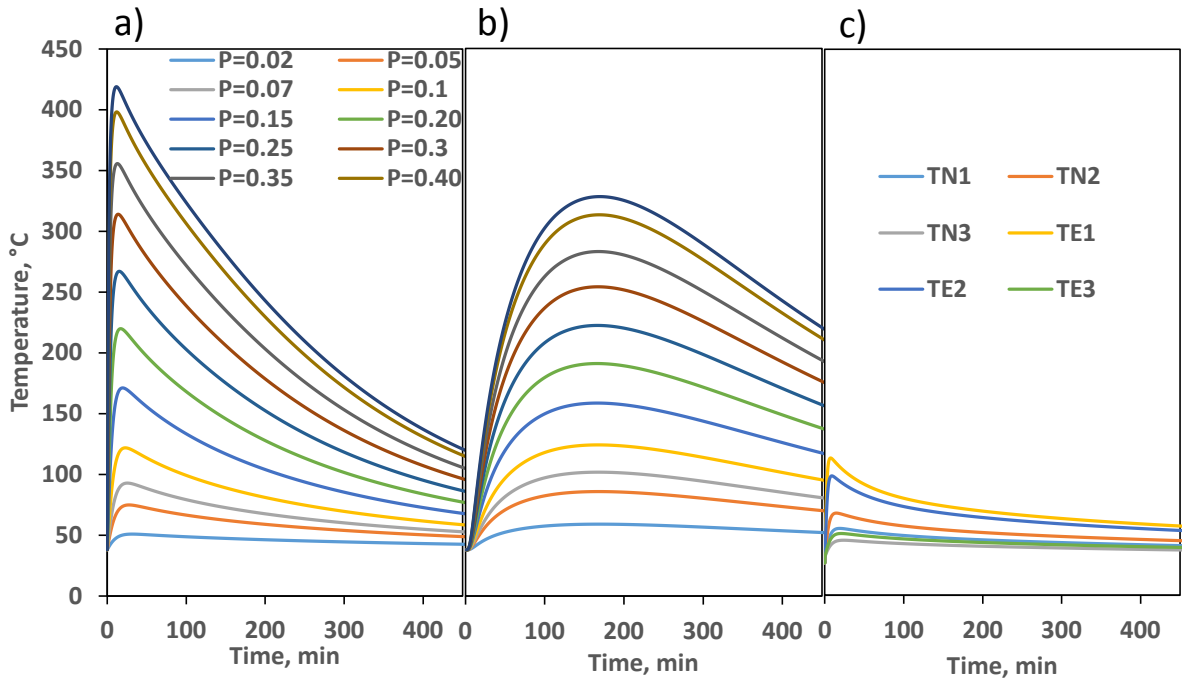

Figure 17: Temperature Profiles as a Function of Time and Energy Deposited in the Fuel Assemblies for the Assumed LEU Core. a) Gas phase temperatures exiting the cooling channels, b) Temperature of the alignment pin, c) Average temperatures entering the radial slots of the grid plate (see Figure 13 for location)

The average energy can be related to specific locations of the fuel assemblies within the core, as shown in the Appendix. Initially, the grid plate is heated by convection through the flow holes, but, eventually, heat conducted axially through the assemblies becomes an important mechanism for heat transfer to the plate. The gas-phase temperature entering the radial slots is lower, thus keeping the sides of the plate cooler.

Temperature profiles for the grid-plate were also calculated for constant power operation at 120 kW. At 4h of operation, the maximum temperature for the LEU core reached ~110 °C. These results (see the Appendix, which also includes corresponding results for the HEU core) were provided to INL for seismic analyses. [Results were not provided for the design-basis accident (DBA), as the likelihood of a DBA coinciding with a design basis earthquake was below the probability threshold of consideration, as per guidance provided in the HEU FSAR]. The effect of thermal expansion and corresponding bowing of the control rod thimbles is discussed in the structural analysis section of this report.

Filtration/Cooling System

Last, the adiabatic temperature of the reactor effluent air to the exhaust filtration system was calculated for the reactivity accident scenario for the LEU and HEU cores. For the HEU core, the effluent air temperature remained below 180 °C even when using one blower only for cooling (assuming nominal operation at 3000 cfm). The analysis for the LEU core showed that nominal flow without use of bypass air from the subpile room will violate the filtration/cooling system temperature limits identified in the HEU FSAR, as shown in Figure 18.

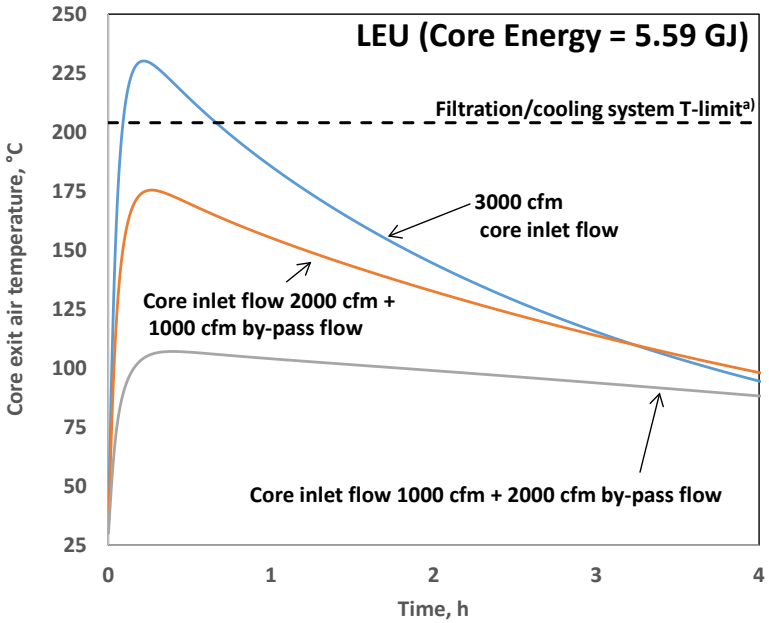

Figure 18: Reactor Effluent Air to the Exhaust Filtration System

With only one blower in operation, the exhaust temperature exceeds the HEU FSAR limit (204°C) for the exhaust filter for a little less than 1h during the transient. During that time, it would be necessary to by-pass some of the flow in order to reduce the gas phase temperature by mixing some of the air flowing out of the core with relatively cold air from the bypass. With 1000 cfm through the core and the reminder of the flow by-passed, the core exit temperature would be below the temperature limit for the exhaust filter with significant margin. However, coolant flow through the core would be reduced, so the temperature of the grid plate is likely to increase (the temperature of the grid plate was not calculated for this scenario). Increasing the flow through the core to 2000 cfm (with 1000 cfm in the bypass) provided a margin of 30 °C to meet the filtration temperature limit. In this case, additional analyses would be required to balance core and bypass flow while satisfying the filtration/cooling system temperature limits with sufficient margin.

4.2.5 Summary

The ancillary radial reflector and grid plate thermal hydraulic analysis was conducted both for an HEU and LEU core (Variant 2.1). For all analyses conducted, the half-slotted core loading of the M8 power calibration experiment (M8CAL) was used.

Given the large thermal mass of the permanent reflector, the reflector is able to absorb a large amount of energy, yet remain sufficiently cool. With adequate cooling, the peak temperature of the permanent reflector remains below 60 °C. This analysis considered that the reflector is heated only from the heat transferred from the adjacent fuel elements. The energy deposition in the permanent reflector from neutrons and photons was not included in this analysis and is subject to consideration in future work.

In support of structural analyses, the grid plate temperature profiles during a bounding accident scenario as well as for constant power operation at 120 kW were evaluated. Calculations for a reactivity accident scenario and with one blower in operation (3000 cfm of air cooling) resulted in the most severe heating of the plate. Because of the higher core energy in the LEU Variant 2.1 core accident case, the grid plate

reaches ~290 °C compared to 170 °C for the HEU core. Since the hottest fuel assemblies are located at the center of the grid plate, the central part of the grid plate reaches much higher temperatures than the outer peripheral region. Temperature profiles for the grid plate were also calculated for constant power operation at 120 kW. At 4h of operation, the maximum temperature for the LEU Variant 2.1 core reached ~110 °C.

4.3 Grid Plate Thermal Distortion

The purpose of the analysis presented here is to determine if particular accident conditions in a TREAT LEU core could lead to excessive thermal distortion in the grid plate, which supports the fuel assemblies. Excessive grid plate distortion could cause the control rods to bind, preventing their operation. Additionally, this analysis seeks to determine the maximum tolerable uniform temperature in the grid plate that would result in a thermal distortion large enough to potentially cause control rod binding. The analysis starts with a finite element model in ANSYS [27] for structural analysis of the grid plate, and uses the weight of fuel assemblies and a non-uniform thermal load calculated separately in COMSOL [28]. The displacement results are then used to determine an angular deflection that occurs at the middle bearing of a control rod. This angular displacement is then applied to a separate ANSYS beam model of the control rod to calculate deflections, which are compared to the clearances in the guide tube and seal assembly. This method is repeated using a uniform thermal load to determine the maximum tolerable temperature for the grid plate.

This analysis was completed using the Variant 2.1 iteration of the LEU core design as a reference. This assessment is considered bounding for any core design that is expected to produce peak fuel temperatures below those produced for the variant referenced in this particular analysis. A description of similar analyses completed and discussions of this topic for the HEU core can be found in Sections 4.3.2.4 and 4.5.6.4 of the HEU FSAR.

4.3.1 Assumptions

This model assumes material properties equivalent to A36 structural steel. The TREAT historical drawings specify mild steel, and Sect III of the ASME Boiler and Pressure Vessel Code lists A36 steel as a typical mild steel. Mechanical properties were obtained from the pressure vessel code and are summarized in Table 12.

The concrete supporting the grid plate is assumed to undergo no significant change in temperature, and thus exhibits no distortion due to thermal loading. The concrete is represented in the ANSYS model by the boundary conditions shown in Figure 20. Also, the weight of a single fuel assembly is assumed to be 100 lbs as a simple static load. Mechanical interaction between the two is assumed only insofar as the grid plate forces the bottom of the control rod assembly to be at the same lateral position as the assembly's hole in the grid plate. (In reality, the fuel assemblies are collectively clamped together at their tops with clamps secured to the concrete shielding of the reactor. On the other hand, the fuel assemblies may distort during transients, due to lateral temperature gradients across them.)

Table 12: Material Properties for A36 Steel

Property	Units	Value
Density	kg/m^3	7850
Young's Modulus	GPa	200
Poisson's Ratio	-	2.6
Coefficient of Thermal Expansion (CTE)	K^{-1}	12.0E-6

4.3.2 Non-Uniform Thermal Loading

This subsection provides details on the analysis of grid plate deflection in the case of non-uniform thermal loading. This loading is assumed to be the result of a bounding reactivity insertion accident with active cooling (i.e. blowers operating at the nominal capacity). In the case of thermal loading on the grid plate, use of blowers provides the most conservative assessment, since heat will transfer to the grid plate more rapidly via convective heat transfer.

4.3.2.1 Geometry of Grid Plate and Control Rods

The grid plate, shown in Figure 19, is supported both by the seal assemblies and the surrounding concrete. The plate rests on the edges of the concrete, which are reinforced with steel. The seal assemblies and the grid plate are bolted together. The grid plate model uses quarter symmetry, and the quarter symmetric model supports 91 fuel assemblies.

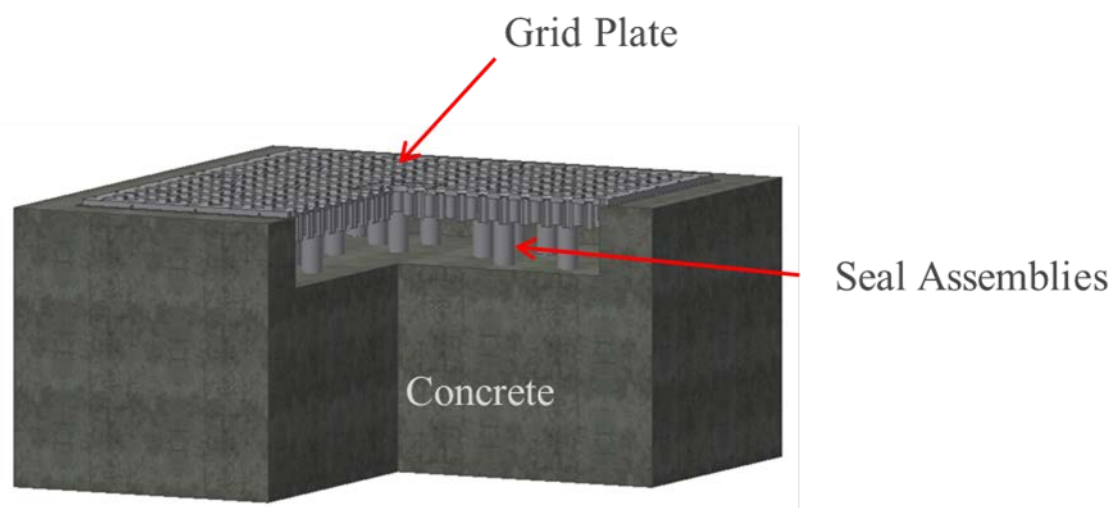

Figure 19: Drawing of Grid Plate and Seal Assemblies

The control rod geometry, shown in Figure 20, used in the ANSYS model takes into account the outer wall of the control rod modeled as a simple beam supported at three locations that correspond to the three graphite bearings, shown in red in the figure. The calculated angular displacement will be enforced at the location of the middle bearing.

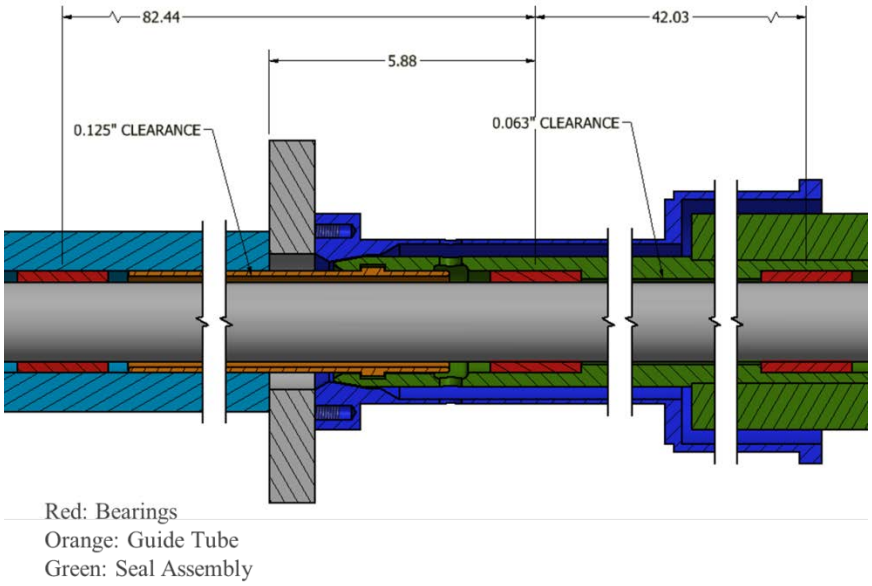

Figure 20: Cross-Sectional View of Control Rod Assembly Showing Graphite Bearings (Red)

4.3.2.2 Grid Plate Boundary Conditions

Non-thermal loading of the grid plate is assumed to be the result of the force imposed by the weight of the assemblies, and the force resulting from contact with support structures. In the case of the fuel assemblies, it is assumed that each assembly weighs 100 lbs. Compression-only support occurs at the edge of the grid plate, where the grid plate is supported along the edge but is not clamped. Additionally, there are fixed supports on the region of the fuel assemblies that are below the surface of the concrete. These loads are shown in the quarter symmetry drawings shown in Figure 21a) and Figure 21b), where the load due to the weight of 91 fuel assemblies is shown in panel a), and the loads resulting from the compression and fixed supports are shown in panel b).

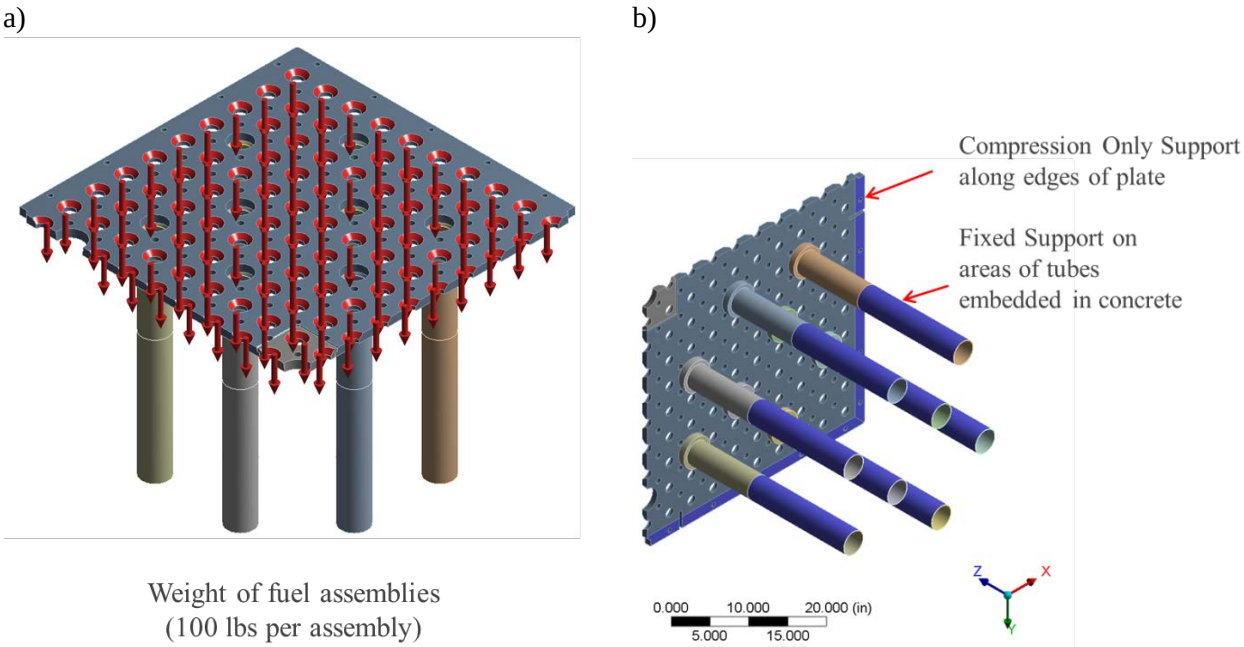

Figure 21: Non-Thermal Grid Plate Loads in the Quarter Symmetry Model

4.3.2.3 Non-Uniform Temperature Distribution

The non-uniform grid plate temperature profile (Figure 22) used in this structural analysis was generated by a thermal hydraulic analysis performed in COMSOL [28]. The thermal-hydraulic model used the half-slotted core loading of the M8 power calibration experiment (M8CAL) with Variant 2.1 LEU fuel assemblies. The reactor is assumed to be convectively cooled by air forced axially downward at a flow rate of 3000 cfm. The accident scenario assumes that all of the reactivity available at the beginning of the planned bounding shaped transient is inserted as a step. The methodology and results of the thermal hydraulic model are discussed in detail in the thermal-hydraulic analysis section of this report.

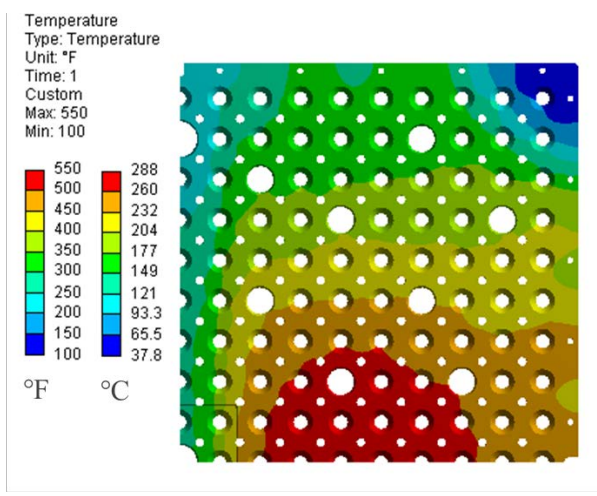

Figure 22: Contour Plot of Non-Uniform Thermal Loading of the Grid Plate in the Design Basis Accident [28]

4.3.2.4 Grid Plate Deflection Due to Non-Uniform Thermal Load

Results for deflection in the grid plate due to non-uniform thermal loading is shown in Figure 23a) and Figure 23b), below. The total deformation for all directions is shown in panel a), and deformation only in the radial direction with respect to the center of the grid plate is shown in panel b).

a) b)

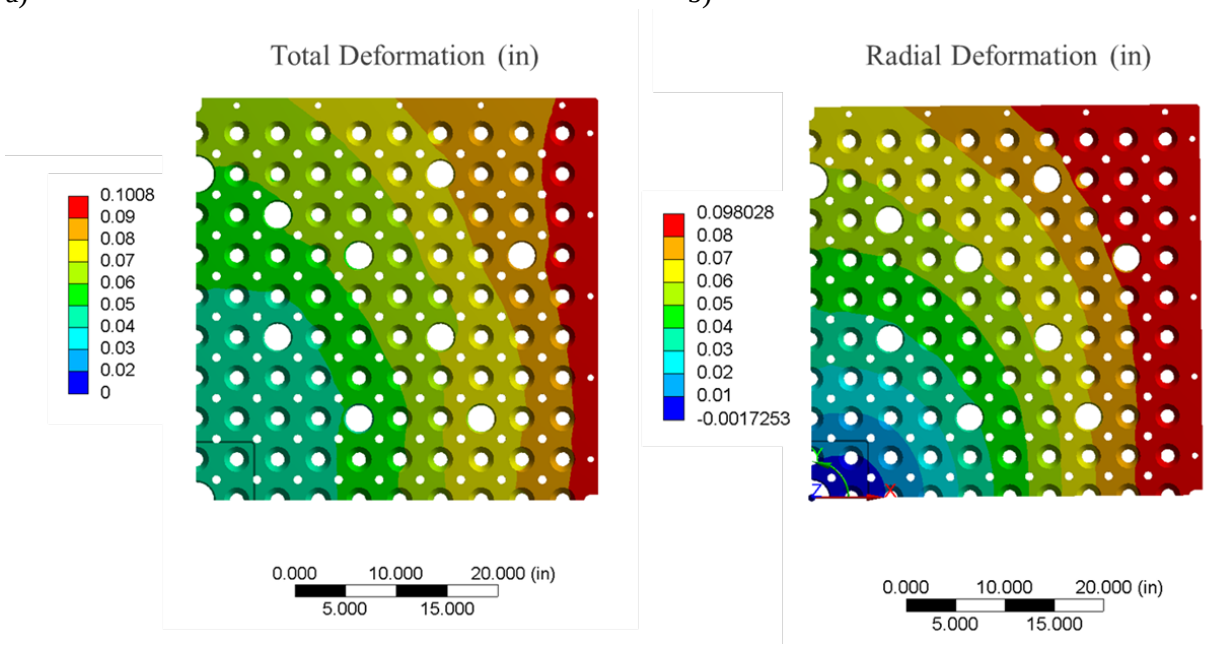

Figure 23: Contour Plots Showing Total (a) and Radial (b) Deformation of the Grid Plate Due to Non-Uniform Thermal Loading

The total deflection from the original position for two control rod positions was also calculated. For a control rod relatively near the axis of symmetry (shown in Figure 24, indicated by the lower red circle), the total deflection is 0.065”. This leads to an angular displacement of 0.31° at the middle bearing of the control rod. The displacement angle is calculated as the arctangent of the deflection divided by 12”, where 12” is the distance between the grid plate and intersection point of the seal assemblies with concrete. For reference, the deflection at a location further from the axis of symmetry (upper red circle in Figure 24) was also assessed, and was found to be 0.086”, leading to a total angular displacement of 0.411°. However, this location is not expected to hold a control rod.

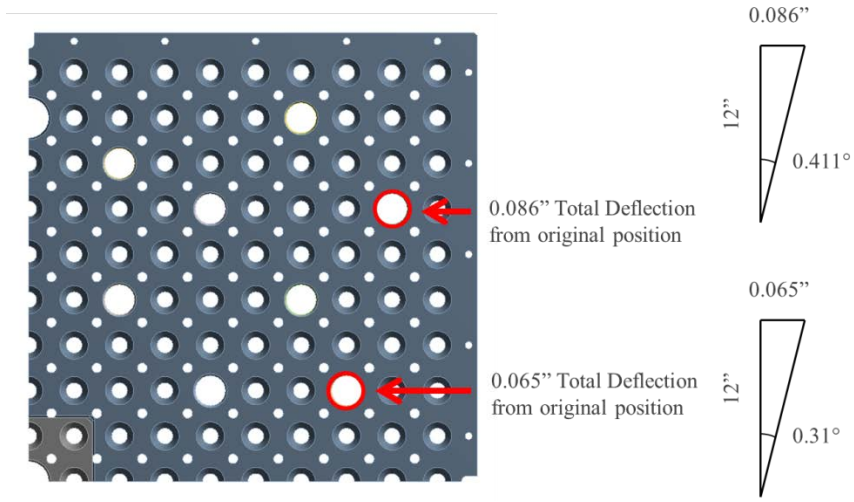

Figure 24: Deflection of Control Rod Positions

4.3.2.5 Control Rod Deflection Due to Non-Uniform Thermal Load

By enforcing an angular displacement of 0.31° at the middle bearing, deflection of the control rod due to non-uniform thermal loading was found to be 0.0863” within the guide tube and 0.044” within the seal assembly, as shown in Figure 25. The clearance in the guide tube is 0.125” and the clearance in the seal assembly is 0.063”. Therefore, the total deflection in the control rods is not expected to result in loss of control rod functionality.

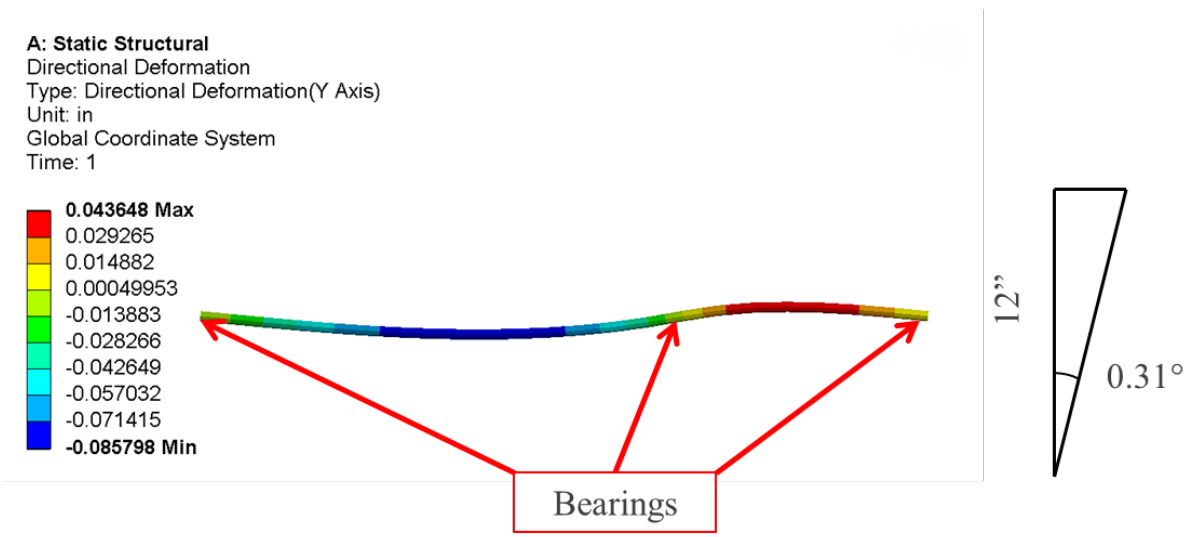

Figure 25: Control Rod Deflection Resulting from 0.31° Angular Displacement at Middle Bearing

4.3.3 Maximum Uniform Temperature

Since the accident scenario used to calculate the thermal loading used in the first analysis did not indicate that the control rods would bind, an additional analysis was performed to determine a maximum uniform thermal load that would cause distortion in the control rods that is equal to or greater than the clearances in the guide tube and seal assembly. The models for both the grid plate and the control rod are the same as the previous analyses with the exception of a uniform temperature applied to the grid plate as shown in

Figure 26. A number of iterations of this analysis were performed to obtain the value for the maximum temperature. As discussed in the following subsections, the final maximum grid plate temperature that would yield grid plate deflection sufficient to induce control rod binding was found to be 320°C.

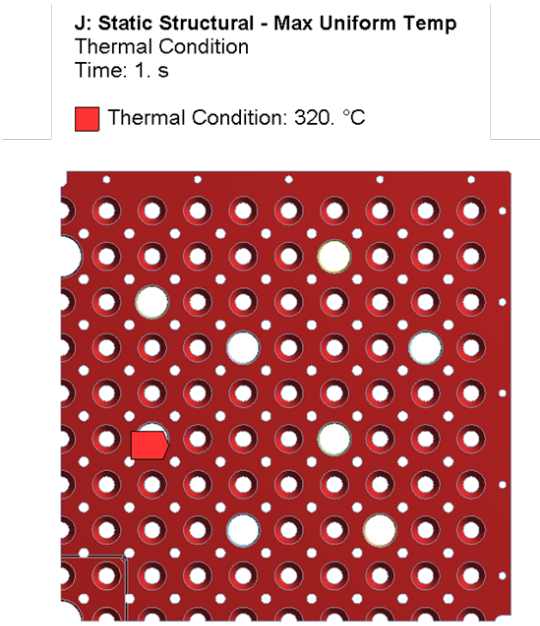

Figure 26: Contour Plot Showing Uniform Grid Plate Temperature of 320 °C

4.3.3.1 Grid Plate Deflection Due to Maximum Uniform Thermal Load

An iterative procedure was used to determine the maximum uniform thermal load required to induce control rod binding from grid plate deflection. For this case, the total deflection of the reference control rod position was found to be 0.093”, resulting in an angular displacement of 0.443° at the middle bearing. A contour plot showing the radial deformation resulting from the uniform grid plate temperature of 320°C is shown in Figure 27a), and the total displacement is shown in Figure 27b).

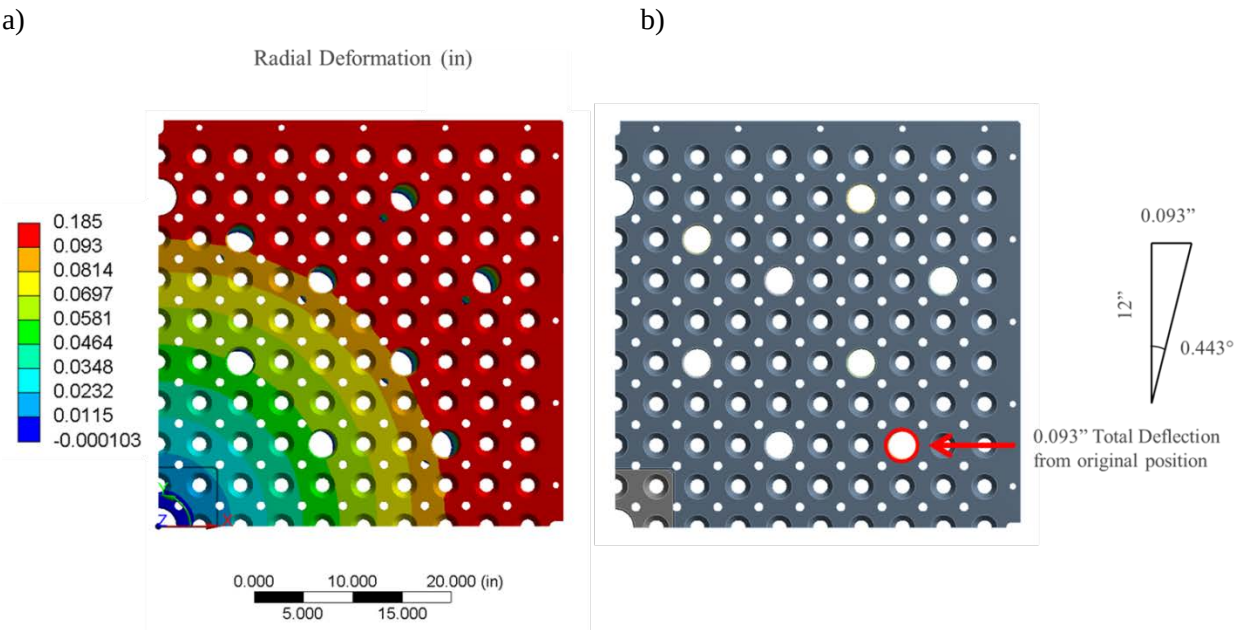

Figure 27: Radial Deformation (a) and Total Deflection (b) Resulting From Uniform Thermal Load of 320°C

4.3.3.2 Control Rod Deflection Due to Maximum Uniform Thermal Load

By enforcing an angular displacement of 0.443° at the middle bearing, deflection of the control rod due to a uniform thermal loading of 320°C was found to approximately meet or exceed the clearance in the guide tube and seal assembly. As shown in Figure 28, the deflection in the guide tube under uniform thermal loading was found to be 0.123”, and the deflection in the seal assembly was found to be 0.0624”, where the clearances in the guide tube and seal assembly are 0.125” and 0.063”, respectively.

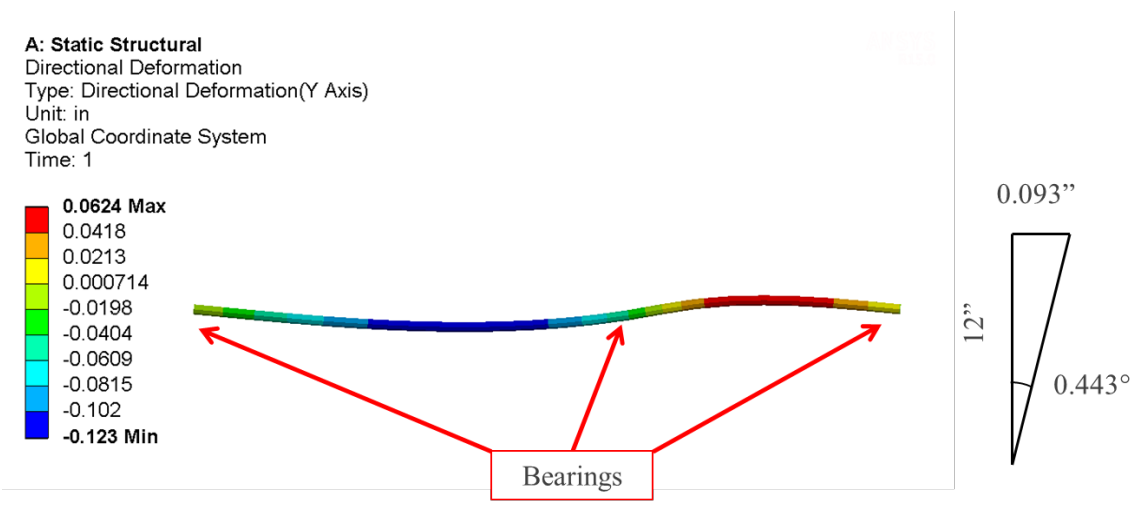

Figure 28: Control Rod Deflection Resulting from 0.443° Angular Displacement at Middle Bearing

4.3.4 Summary

Analysis of the control rod deflection for an accident case with an LEU core shows that the control rods will not deflect enough to cause binding with either the guide tube or seal assembly.

Analysis of grid plate with a uniform thermal load was completed, demonstrating that a uniform temperature in the grid plate beyond 320 °C brings the control rod into contact with the seal assembly and the guide tube. Thermal distortion of the guide tubes has not been calculated but could also contribute to binding of the control rods.

5. Ongoing and Future Ancillary Safety Analyses

Concurrent with ongoing LEU fuel design activities and supplemental thermal hydraulic analyses, additional ancillary safety analyses are either in the process of being completed or will be completed once the fuel design has achieved a higher maturity. The majority of these tasks are related to additional shielding or neutronic analyses, where results obtained using the current LEU design will be compared to those obtained using Argonne's HEU MCNP model or to historical data and documentation. The methodologies utilized for these analyses are consistent with, or improved from, those utilized for HEU analyses in the SAR. A brief description of the ongoing and future safety analyses is below.

- **Dose rates at periphery of biological shield**
  Dose rates at the outer edge of the biological shield will be assessed during normal operating conditions and post-transient, including during steady state operation and at 16 hr and 24 hr following a large transient test. The dose will be determined at the radial periphery of the shield, at the top and bottom of the removable shield blocks, and at the bottom of the biological shield, which is considered to be the subpile room ceiling. Hot-spot locations due to penetrations through the shielding will be considered. This analysis is currently ongoing.
- **Dose rates at periphery of radiography facility**
  A radiography facility at the west face of the reactor allows for pre- and post-transient imaging of tests. The expected dose rate will be assessed near this facility, at the outer edge of the facility's radial shield, and at the center of the beamline. Doses will be tabulated during steady state operation. This analysis is currently ongoing.
- **Dose rate in subpile room from control rod followers**
  The control rod followers, which are located near the lower end of the bottom-inserted control rods, directly experience flux when the rods are fully inserted, and therefore become activated. During steady state operation and transient testing, the followers are not enclosed by shielding and are partially exposed in the subpile room. The doses from the activated followers at various locations in the subpile room will be assessed for steady state operation and at multiple time periods following a large transient test. This analysis currently ongoing.
- **Thermal distortion of control rods due to localized hot spots and asymmetric heating**
  There is the potential for control rod bowing and other thermally-induced mechanical distortion as the result of radially asymmetric heating of control rods. This distortion may be significant enough such that control rod motion is degraded or prevented. Efforts to determine the maximum possible asymmetric heating that can occur before unacceptable mechanical distortion occurs is currently ongoing.
- **Accidental criticality due to flooding**
  The potential for criticality due to hypothetical flooding of the reactor was evaluated in the HEU FSAR, and is also being evaluated for the LEU core for completeness. The preliminary results, which are currently undergoing additional technical review, indicate that there is no danger of criticality due to complete flooding of the reactor with rods fully inserted.
- **Coolant activation**
  Activation of coolant in TREAT is an important issue due to the filtered, open-loop cooling system. Coolant activation, which in the case of TREAT is air, can lead to an activated effluent release from the exhaust stack or deposition in the HEPA filter banks. A preliminary assessment of coolant activation has been performed, and is currently undergoing technical review. This analysis also includes an assessment of the potential effects of blower speed on air activation.

- **Effect of heat transfer between test vehicle and TREAT core**
  Because of the historic need to limit the peak temperature in the fuel assembly, the potential for additional heat transfer from in-core experiment hardware to adjacent TREAT fuel assemblies must be considered. As discussed in Section 4.1, this topic will be revisited once the LEU design has reached the conceptual stage.
- **Adequacy of plant protection system**
  The plant protection system at TREAT is not expected to undergo any revisions or modifications as part of the conversion project. Therefore, the existing control system must be able to shut down the core, and in the case of unplanned transients, the trip system must be able to preclude the occurrence of fuel temperatures above the designated safety limit. An analysis will be performed in which the adequacy of the control rod drop time, including trip signal and control system time constant delays, will be assessed taking into account the difference between the neutronic differences between the HEU and LEU cores during fast power transients.

6. Conclusions

In support of TREAT LEU conversion efforts, various ancillary safety analyses have been performed to evaluate whether the LEU core will perform within the operating envelope of facility's support systems and whether established safety limits will be satisfied. Preliminary shielding, neutronic, and thermal hydraulic analyses have been completed and have generally demonstrated that the LEU core will satisfy existing safety limits and standards also satisfied by the existing HEU core. These analyses include the assessment of the dose rate in the hodoscope room, near a loaded fuel transfer cask, above the storage area, and near the HEPA filters. The potential change in the concentration of tramp uranium and change in neutron flux reaching instrumentation has also been assessed. Safety-significant thermal hydraulic items addressed in this report include thermally-induced mechanical distortion of the grid plate, and heating in the radial reflector. Future and ongoing ancillary safety analyses have also been identified and described in this report. The majority of these analyses will proceed concurrently with revisions to the LEU design, although some ancillary analyses (e.g. assessment of the adequacy of the plant protection system) will not begin until the LEU design has achieved higher maturity. Methodologies similar to those utilized in the HEU FSAR have been applied for most analyses where appropriate; however, updated or improved analysis techniques have been utilized for the LEU analyses when possible.

All analyses described in this report have been reviewed for technical content and are considered to be complete, although preliminary. As the LEU design approaches its final stages of maturity, all ancillary safety analyses will be reviewed to determine if the previous analyses can be considered bounding. For any analysis not identified as bounding or conservative, the item will be revisited using the latest LEU design, and additional analyses will be completed. Given the relative progression of the LEU fuel design [4]), it is anticipated that most of the analyses presented here will be bounding.

Works Cited

[1] Idaho National Laboratory, "TREAT LEU Conversion Safety Requirements and Analysis Work Plan Basis," Idaho National Laboratory, Unpublished Information 2013.

[2] Idaho National Laboratory, "Facility Impact Scoping Assessment for Conversion of TREAT to LEU Fuel," Idaho National Laboratory, Unpublished Information 2014.

[3] Idaho National Laboratory, "Transient Reactor Test Facility (TREAT) FSAR, Rev. 7," Idaho National Laboratory, Unpublished Information 2009.

[4] H. M. Connaway, D. C. Kontogeorgakos, D. D. Papadias, and A. E. Wright, "Overview and Current Status of Analyses of Potential LEU Design Concepts for TREAT," Argonne National Laboratory, ANL/RTR/TM-15/9, 2015.

[5] G. A. Freund, P. Elias, D. R. MacFarlane, and J. D. Geier, "Design Summary Report on the Transient Reactor Test Facility (TREAT)," Argonne National Laboratory, ANL-6034, 1960.

[6] D. C. Kontogeorgakos, H. M. Connaway, G. Yesilyurt, and A. E. Wright, "Neutronics Analysis of the Minimum Original HEU TREAT Core," Argonne National Laboratory, ANL/GTRI/TM-14/13, 2014.

[7] D. Kontogeorgakos, K. Derstine, A. Wright, T. Bauer, and J. Stevens, "Initial Neutronics Analyses for HEU to LEU Fuel Conversion of the Transient Reactor Test Facility (TREAT) at the Idaho National Laboratory," Argonne National Laboratory, ANL/GTRI/TM-13/4, 2013.

[8] ASTM Standard B350/B350M-11, "Standard Specification for Zirconium and Zirconium Alloy Ingots for Nuclear Application," ASTM International, 2011.

[9] R. W. Swanson, "Annual Radioactive Nuclide Emissions from the TREAT Stack," Argonne National Laboratory, Unpublished Information, 1992.

[10] R. J. Cornella, "HEPA Filter Loading Calculations," Argonne National Laboratory, Unpublished Information 1982.

[11] S. Yang, "Dose Rate in Hodoscope Room and Mezzanine Level Due to HEPA Filters," Argonne National Laboratory, Unpublished Information 1983.

[12] Persional communication with G. Yesilyurt, Argonne National Laboratory, Sept. 24, 2014.

[13] J. T. Goorley, et al., "Initial MCNP6 Release Overview - MCNP6 version 1.0," LA-UR-13-22934, 2013.

[14] Personal communication with E. Hoffman, Argonne National Laboratory, 2014.

[15] Code of Federal Regulations, "Standards for Protection Against Radiation," 10CFR20, Ammended 2014.

[16] International Commission on Radiological Protection, "1990 Recommendations of the International Commission on Radiological Protection," ICRP Pub. 60, Ann. ICRP 21 (1-3), 1991.

[17] Personal communication with G. Yesilyurt, Argonne National Laboratory, 2014.

[18] J. Cetnar, J. Wallenius, and W. Gudowski, "MCB: A Continuous Energy Monte Carlo Burnup Simulation Code, MCB User Manual - V1.0," KTH Royal Institute of Technology, Retrieved from http://www.neutron.kth.se/research/MCB/MCBmanual.shtml, 2015.

[19] A. G. Croff, "A User's Manual for the ORIGEN2 Computer Code," Oak Ridge National Laboratory, ORNL/TM-7175, 1980.

[20] ANS-6.1.1 Working Group, "American National Standard Neutron and Gamma-Ray Flux-to-Dose Rate Factors," American Nuclear Society, ANSI/ANS-6.1.1-1997(N666), 1977.

[21] T. Fei, "Photon Dose Rate Evaluation Around a Loaded TREAT Fuel Transfer Cask," Argonne National Laboratory, Unpublished Information, 2014.

[22] W. R. Robinson and T. H. Bauer, "The M8 Power Calibration Experiment (M8CAL)," Argonne National Laboratory, ANL-IFR-232, 1994.

[23] D. Papadias and A. Wright, "Thermal Analysis of a TREAT Fuel Assembly," Argonne National Laboratory, ANL/GTRI/TM-14/14, 2014.

[24] D. C. Kontogeorgakos, H. M. Connaway, and A. E. Wright, "Temperature Dependence of Test Fuel Power Density and Core Energy During Transient Reactor Test Facility (TREAT) Irradiation Experiments," in *Transactions of the American Nuclear Society*, vol. 112, San Antonio, TX, June 7-11, 2015, pp. 363-366.

[25] Personal communication with H. M. Connaway, Argonne National Laboratory, 2014.

[26] D. R. Ramaswami, Unpublished Information, 1982.

[27] ANSYS, Inc., "ANSYS, Vers. 16.2," ANSYS, Inc., 2015.

[28] Personal communication with D. D. Papadias, Argonne National Laboratory, 2014.

[29] Personal communication with D. C. Kontogeorgakos, Argonne National Laboratory, 2015.

Appendix A

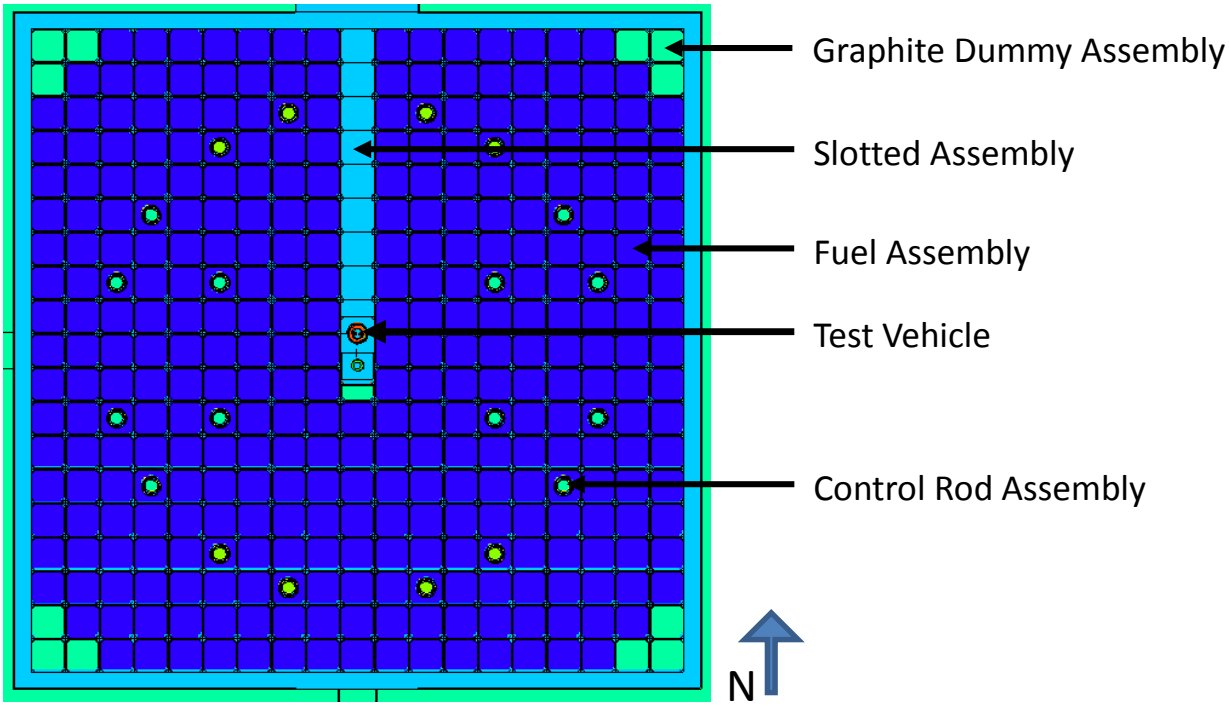

Figure A - 1: Cross-Section View of MCNP Model of the M8CAL Experiment Core Loading [25]

During the M8CAL experiments, fuel assemblies were not utilized in all of the possible locations in the core. Each corner had three graphite dummy assemblies, which contained plain graphite rather than the UO_2-graphite mixture of the fuel. The experiment vehicle was placed in the center of the core, with a half-sized graphite assembly behind it. In the north direction, "slotted" assemblies extended from the center of the core that provided an air channel for viewing access from the core edge to the core center.

	HEU Fuel Assembly power divided by total core power (cold core w/ control/shutdow rods partially inserted)																		
	Relative to total power (for T/H)																		
	A	B	C	D	E	F	G	H	J	K	L	M	N	O	P	R	S	T	U
1			0.00173	0.00170	0.00168	0.00162	0.00152	0.00138	0.00133		0.00132	0.00137	0.00151	0.00161	0.00165	0.00168	0.00174		
2		0.00186	0.00183	0.00182	0.00179	0.00172	0.00161	0.00150	0.00153		0.00153	0.00150	0.00162	0.00173	0.00180	0.00184	0.00187	0.00194	
3	0.00197	0.00196	0.00202	0.00205	0.00199	0.00185	0.00177	0.00110	0.00174		0.00174	0.00111	0.00178	0.00187	0.00202	0.00210	0.00209	0.00207	0.00213
4	0.00209	0.00215	0.00228	0.00235	0.00224	0.00137	0.00211	0.00212	0.00211		0.00211	0.00214	0.00214	0.00139	0.00229	0.00242	0.00237	0.00229	0.00230
5	0.00230	0.00239	0.00257	0.00269	0.00269	0.00263	0.00266	0.00262	0.00247		0.00248	0.00265	0.00269	0.00268	0.00276	0.00277	0.00268	0.00254	0.00251
6	0.00253	0.00264	0.00284	0.00209	0.00313	0.00318	0.00315	0.00302	0.00276		0.00277	0.00305	0.00319	0.00324	0.00322	0.00216	0.00297	0.00280	0.00273
7	0.00273	0.00287	0.00310	0.00333	0.00350	0.00356	0.00351	0.00331	0.00293		0.00294	0.00334	0.00356	0.00364	0.00359	0.00344	0.00323	0.00302	0.00293
8	0.00291	0.00306	0.00231	0.00359	0.00379	0.00267	0.00377	0.00349	0.00294		0.00296	0.00352	0.00382	0.00272	0.00388	0.00371	0.00239	0.00320	0.00309
9	0.00304	0.00321	0.00351	0.00381	0.00402	0.00408	0.00398	0.00360	0.00278		0.00280	0.00364	0.00404	0.00416	0.00412	0.00392	0.00364	0.00335	0.00321
10	0.00312	0.00330	0.00362	0.00394	0.00417	0.00426	0.00416	0.00377	0.00283		0.00285	0.00381	0.00422	0.00434	0.00428	0.00406	0.00375	0.00344	0.00329
11	0.00314	0.00332	0.00364	0.00397	0.00422	0.00434	0.00430	0.00403	0.00336		0.00338	0.00407	0.00436	0.00442	0.00433	0.00410	0.00377	0.00346	0.00331
12	0.00311	0.00328	0.00249	0.00391	0.00417	0.00301	0.00437	0.00427	0.00403	0.00387	0.00405	0.00432	0.00443	0.00307	0.00428	0.00403	0.00258	0.00341	0.00327
13	0.00302	0.00318	0.00347	0.00377	0.00403	0.00422	0.00433	0.00435	0.00432	0.00429	0.00434	0.00440	0.00439	0.00430	0.00413	0.00389	0.00359	0.00332	0.00318
14	0.00290	0.00303	0.00330	0.00246	0.00376	0.00393	0.00408	0.00420	0.00426	0.00428	0.00428	0.00424	0.00415	0.00401	0.00386	0.00254	0.00342	0.00317	0.00305
15	0.00274	0.00285	0.00307	0.00326	0.00334	0.00338	0.00360	0.00381	0.00394	0.00400	0.00396	0.00385	0.00366	0.00346	0.00344	0.00337	0.00318	0.00297	0.00289
16	0.00257	0.00263	0.00281	0.00294	0.00288	0.00183	0.00299	0.00320	0.00344	0.00356	0.00346	0.00324	0.00305	0.00188	0.00297	0.00305	0.00292	0.00276	0.00271
17	0.00244	0.00245	0.00255	0.00264	0.00264	0.00259	0.00261	0.00174	0.00293	0.00311	0.00294	0.00177	0.00266	0.00266	0.00274	0.00276	0.00267	0.00258	0.00259
18		0.00235	0.00234	0.00239	0.00245	0.00249	0.00250	0.00252	0.00270	0.00280	0.00272	0.00256	0.00257	0.00259	0.00258	0.00253	0.00248	0.00250	
19			0.00225	0.00226	0.00234	0.00243	0.00251	0.00259	0.00267	0.00271	0.00269	0.00264	0.00259	0.00256	0.00251	0.00245	0.00242		

	LEU Fuel Assembly power divided by total core power (cold core w/ control/shutdow rods partially inserted)																		
	Relative to total power (for T/H)																		
	A	B	C	D	E	F	G	H	J	K	L	M	N	O	P	R	S	T	U
1			0.00200	0.00190	0.00185	0.00178	0.00167	0.00151	0.00148		0.00148	0.00151	0.00166	0.00177	0.00184	0.00188	0.00201		
2		0.00208	0.00191	0.00186	0.00181	0.00173	0.00161	0.00151	0.00158		0.00158	0.00151	0.00162	0.00174	0.00183	0.00188	0.00197	0.00218	
3	0.00229	0.00206	0.00203	0.00204	0.00195	0.00180	0.00172	0.00107	0.00176		0.00176	0.00107	0.00174	0.00183	0.00199	0.00210	0.00212	0.00219	0.00249
4	0.00237	0.00220	0.00227	0.00231	0.00218	0.00130	0.00205	0.00208	0.00212		0.00212	0.00210	0.00207	0.00132	0.00224	0.00239	0.00238	0.00237	0.00262
5	0.00257	0.00244	0.00254	0.00263	0.00262	0.00254	0.00258	0.00258	0.00248		0.00249	0.00260	0.00263	0.00260	0.00270	0.00274	0.00268	0.00261	0.00284
6	0.00281	0.00268	0.00282	0.00204	0.00306	0.00309	0.00307	0.00297	0.00276		0.00277	0.00300	0.00312	0.00316	0.00315	0.00212	0.00295	0.00285	0.00306
7	0.00303	0.00290	0.00307	0.00326	0.00341	0.00347	0.00342	0.00325	0.00293		0.00294	0.00329	0.00348	0.00355	0.00351	0.00338	0.00321	0.00307	0.00327
8	0.00321	0.00309	0.00226	0.00351	0.00369	0.00259	0.00368	0.00343	0.00295		0.00297	0.00347	0.00375	0.00265	0.00380	0.00363	0.00236	0.00326	0.00344
9	0.00335	0.00323	0.00345	0.00371	0.00390	0.00397	0.00388	0.00354	0.00280		0.00281	0.00359	0.00395	0.00406	0.00401	0.00384	0.00359	0.00340	0.00358
10	0.00343	0.00332	0.00356	0.00384	0.00404	0.00412	0.00404	0.00369	0.00284		0.00286	0.00374	0.00411	0.00421	0.00415	0.00397	0.00370	0.00349	0.00366
11	0.00346	0.00334	0.00358	0.00386	0.00408	0.00420	0.00416	0.00392	0.00334		0.00336	0.00398	0.00423	0.00428	0.00420	0.00399	0.00371	0.00350	0.00368
12	0.00342	0.00330	0.00242	0.00380	0.00404	0.00288	0.00422	0.00413	0.00393	0.00380	0.00395	0.00418	0.00429	0.00295	0.00415	0.00393	0.00252	0.00346	0.00363
13	0.00333	0.00320	0.00340	0.00366	0.00389	0.00405	0.00414	0.00418	0.00415	0.00413	0.00418	0.00422	0.00422	0.00414	0.00400	0.00379	0.00355	0.00336	0.00354
14	0.00320	0.00306	0.00323	0.00237	0.00362	0.00376	0.00390	0.00401	0.00407	0.00409	0.00409	0.00404	0.00396	0.00385	0.00373	0.00246	0.00337	0.00321	0.00340
15	0.00303	0.00287	0.00301	0.00316	0.00321	0.00322	0.00342	0.00362	0.00375	0.00381	0.00377	0.00366	0.00348	0.00330	0.00331	0.00329	0.00314	0.00301	0.00323
16	0.00287	0.00267	0.00276	0.00285	0.00276	0.00170	0.00282	0.00302	0.00326	0.00338	0.00328	0.00306	0.00288	0.00175	0.00286	0.00297	0.00289	0.00282	0.00306
17	0.00281	0.00254	0.00253	0.00258	0.00255	0.00247	0.00247	0.00162	0.00278	0.00297	0.00280	0.00165	0.00254	0.00255	0.00266	0.00271	0.00268	0.00269	0.00300
18		0.00260	0.00242	0.00241	0.00244	0.00246	0.00246	0.00246	0.00264	0.00275	0.00267	0.00251	0.00254	0.00257	0.00258	0.00257	0.00258	0.00278	
19			0.00257	0.00250	0.00257	0.00265	0.00272	0.00280	0.00288	0.00293	0.00291	0.00286	0.00283	0.00280	0.00276	0.00273	0.00279		

Fuel assembly	Control rod	Transient rod	Compensation rod

Figure A - 2: Fraction of Core Energy Deposition for an Accident Scenario (5.20% reactivity insertion). Total core energy during the transient: HEU = 4.6 GJ, LEU = 5.59 GJ [29].

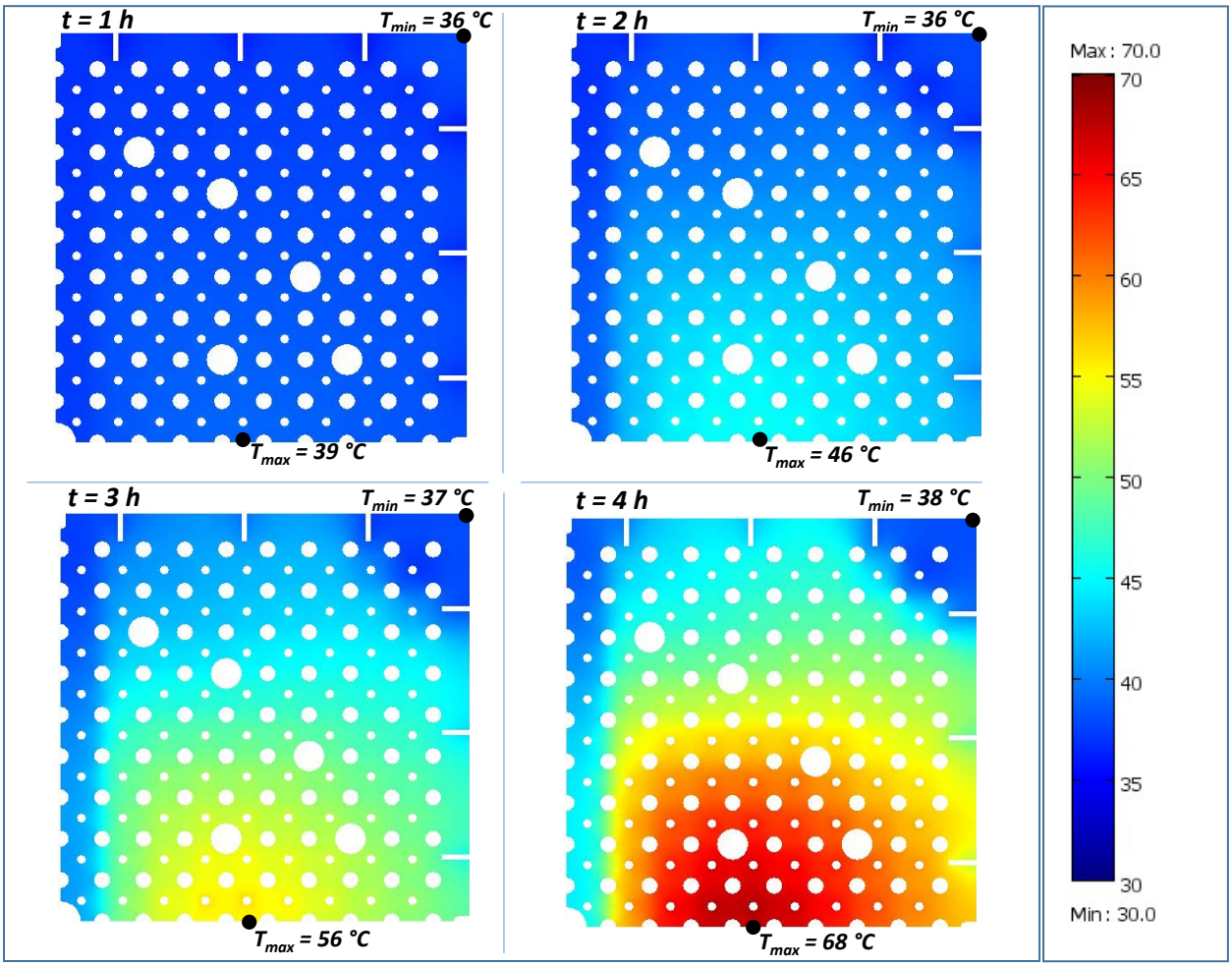

Figure A - 3: Grid Plate Temperature Profiles for HEU core During Steady State Power Operation at 120 kW, Air Coolant Flow Rate = 3000 cfm

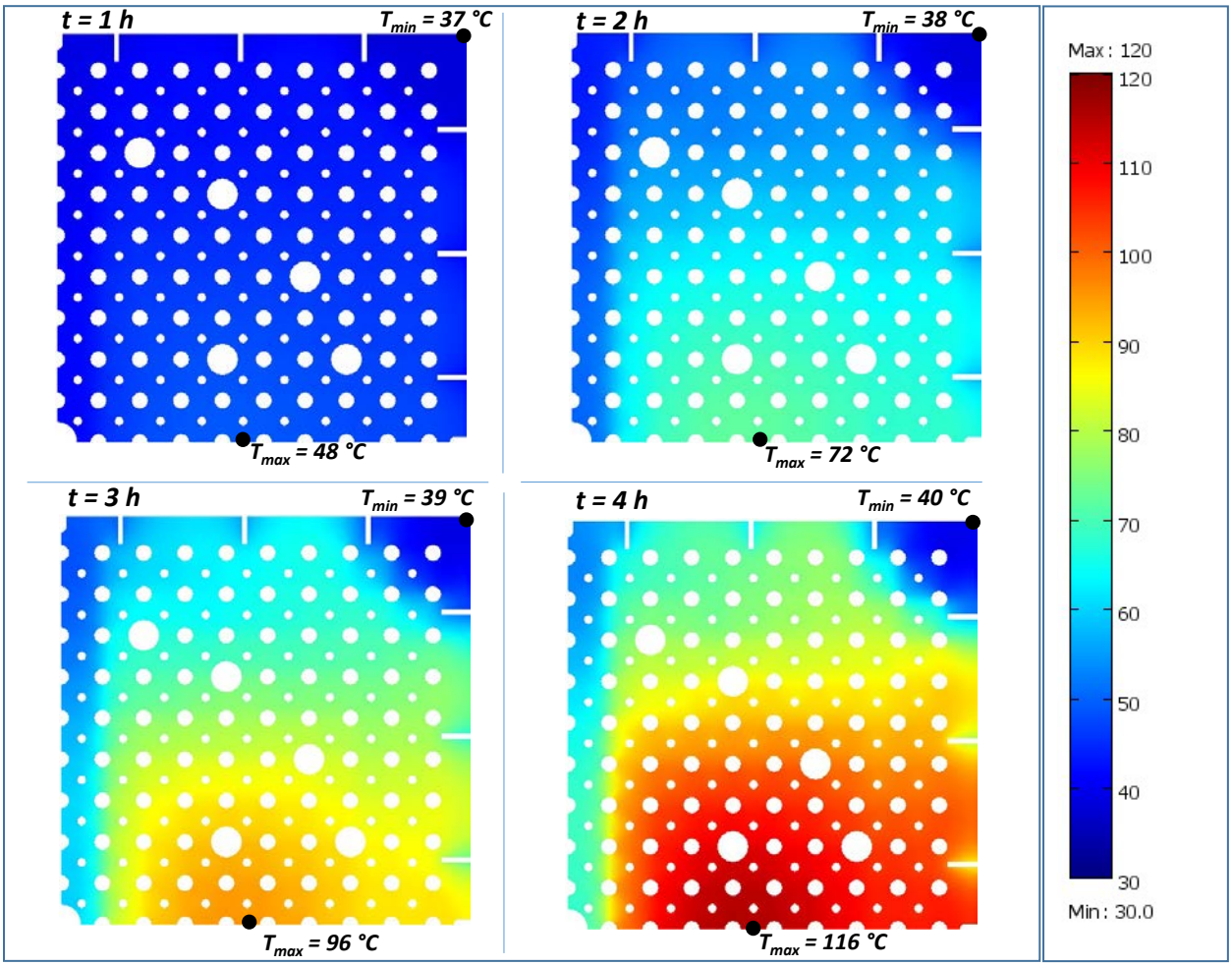

Figure A - 4: Grid Plate Temperature Profiles for LEU Core (Variant 2.1) During Steady State Power Operation at 120 kW, Air Coolant Flow Rate = 3000 cfm

Nuclear Engineering Division
Argonne National Laboratory
9700 South Cass Avenue, Bldg. 208
Argonne, IL 60439-4842

www.anl.gov

Argonne National Laboratory is a U.S. Department of Energy
laboratory managed by UChicago Argonne, LLC